AD-A084 964 GEORGETOWN UNIV WASHINGTON D C DEPT OF PHYSICS F/G 20/1
NONSPECULAR ULTRASONIC EFFECTS FOR LAYERED MEDIA AND SECOND HAR--ETC(U)
APR 80 N G BROWER, D HINDERGER, J A MC/CLURE N00014-78-C-0884
UNCLASSIFIED GUUS-84002 NL

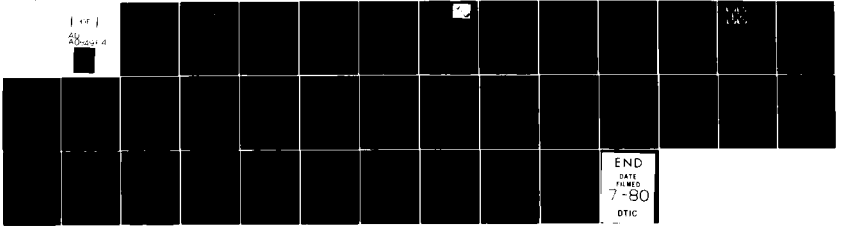

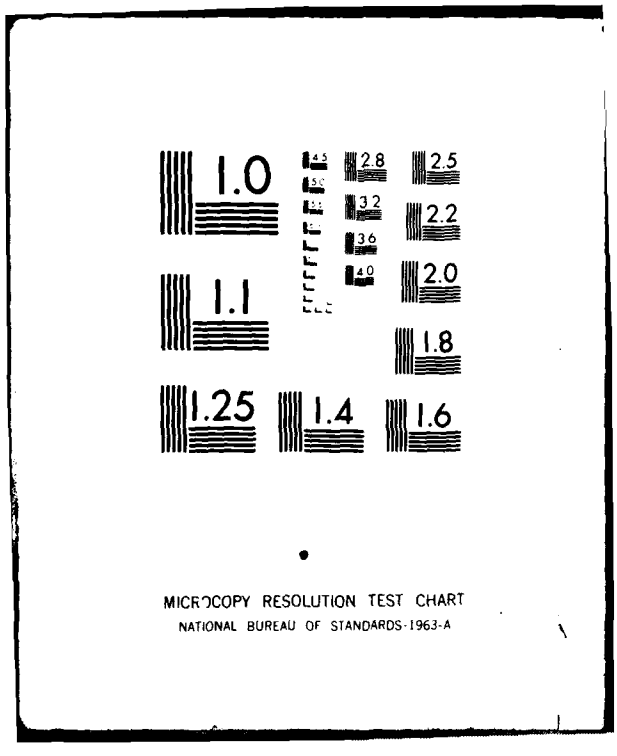
1.0
1.1
1.25
1.4
1.6
1.8
2.0
2.2
2.5
2.8
3.2
3.6
4.0
4.5
5.0
MICROCOPY RESOLUTION TEST CHART
NATIONAL BUREAU OF STANDARDS-1963-A

Office of Naval Research

Contract N00014-78-C-0584

Technical Report No. 2

NONSPECULAR ULTRASONIC EFFECTS FOR LAYERED MEDIA AND SECOND HARMONICS IN LAMB WAVES

by

N. G. Brower, D. E. Himberger, W. G. Mayer

J. A. McClure, K. W. Ng, and T. D. K. Ngoc

Walter G. Mayer
Principal Investigator
Department of Physics
Georgetown University
Washington, DC 20057

April 1980

Unclassified
SECURITY CLASSIFICATION OF THIS PAGE (When Data Entered)

REPORT DOCUMENTATION PAGE	READ INSTRUCTIONS BEFORE COMPLETING FORM
1. REPORT NUMBER: GUUS-04802 (14) (6)	2. GOVT ACCESSION NO.: AD-A084964
3. RECIPIENT'S CATALOG NUMBER: (9)	
4. TITLE (and Subtitle): Nonspecular ultrasonic effects for layered media and second harmonics in Lamb waves.	5. TYPE OF REPORT & PERIOD COVERED: Technical Rept. no. 2 (3) 16 Jul 79 — 1 Apr 80
	6. PERFORMING ORG. REPORT NUMBER: TR-2
7. AUTHOR(s): (10) N. G. Brower, D. Himberger, J. A. McClure, W. G. Mayer, K. W. Ng, D.K. Ngoc. (Walter)	8. CONTRACT OR GRANT NUMBER(s): N0014-78-C-0584 (15)
9. PERFORMING ORGANIZATION NAME AND ADDRESS: Physics Department, Georgetown University, Washington, DC 20057	10. PROGRAM ELEMENT, PROJECT, TASK AREA & WORK UNIT NUMBERS: 121108
11. CONTROLLING OFFICE NAME AND ADDRESS: Office of Naval Research, Code 421, Arlington, VA 22217	12. REPORT DATE: (11) Apr 80
	13. NUMBER OF PAGES: 34 (12) 36
14. MONITORING AGENCY NAME & ADDRESS (if different from Controlling Office)	15. SECURITY CLASS. (of this report): Unclassified
	15a. DECLASSIFICATION/DOWNGRADING SCHEDULE

16. DISTRIBUTION STATEMENT (of this Report)

Approved for public release; distribution unlimited.

17. DISTRIBUTION STATEMENT (of the abstract entered in Block 20, if different from Report)

Approved for public release; distribution unlimited.

18. SUPPLEMENTARY NOTES

19. KEY WORDS (Continue on reverse side if necessary and identify by block number)

Ultrasonics, solid plates, half-space, specular and nonspecular reflectivity and transmissivity, Lamb waves, harmonic generation, Rayleigh waves, acousto-optic interaction.

20. ABSTRACT (Continue on reverse side if necessary and identify by block number)

Theoretical and experimental evidence is given to explain reflectivity and transmissivity of bounded ultrasonic beams impinging on flat solid thin and thick plates immersed in water. Effects are described which have to be considered when high amplitude ultrasonics is used or when the liquid-solid combination differs significantly from the usual metal-water combination of reflecting media.

DD FORM 1 JAN 73 1473 EDITION OF 1 NOV 65 IS OBSOLETE
S/N 0102-014-6601

Unclassified
SECURITY CLASSIFICATION OF THIS PAGE (When Data Entered)

153 620

This Technical Report describes work performed under Contract N00014-78-C-0584 "Linear and Nonlinear Ultrasonic Interactions on Liquid-Solid Boundaries." The Report consists of the following articles:

"Ultrasonic nonspecular reflectivity near longitudinal critical angle" by T.D.K. Ngoc and W.G. Mayer, J. Appl. Phys. 50, 7948 (1979).

"Numerical integration method for reflected beam profiles near Rayleigh angle" by T.D.K. Ngoc and W.G. Mayer, J. Acoust. Soc. Am. 67, No. 4, 1149 (1980).

"Nonspecular transmission effects for ultrasonic beams incident on a solid plate in a liquid" by K.W. Ng, T.D.K. Ngoc, J.A. McClure, and W.G. Mayer, (for publication in ACUSTICA).

"Restrictions on the existence of leaky Rayleigh waves" by N.G. Brower, D.E. Himberger, and W.G. Mayer, IEEE Trans. SU, 26, 306 (1979).

"Acousto-optic interaction of second harmonics in Lamb waves" by N.G. Brower and W.G. Mayer, J. de Physique 40, C8-175 (1979).

The first three of above listed papers describe both theoretical and experimental results which are used to evaluate and explain the reflectivity and transmissivity of bounded ultrasonic beams impinging on flat solid thin or thick plates which are surrounded by water. The angle of incidence of the incident beam determines what type of reflectivity or transmissivity may be expected. The last two papers describe effects which have to be taken into consideration when either high amplitude ultrasonics is used or the liquid-solid combination is changed significantly from the usual parameters describing a normal metal-water boundary.

W. G. Mayer
Principal Investigator

Washington, DC, April 1980

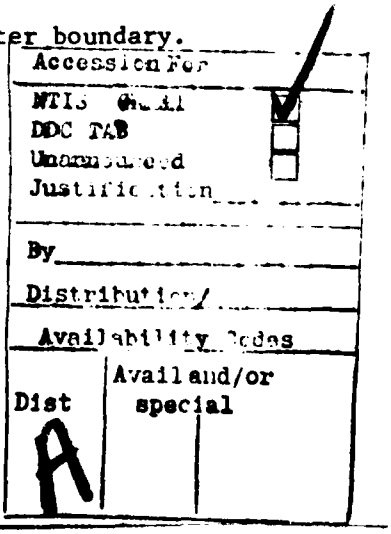

Ultrasonic nonspecular reflectivity near longitudinal critical angle

Tran D. K. Ngoc and Walter G. Mayer
Physics Department, Georgetown University, Washington, D.C. 20057

A numerical integration method is developed to determine the intensity profile of an ultrasonic beam reflected from a liquid-solid interface near the longitudinal critical angle. The profiles are calculated for different combinations of frequencies and beam widths with the angle of incidence being varied about the longitudinal critical angle for a water-Plexiglas interface. These calculations demonstrate the existence of nonspecular reflectivity near this particular critical angle and provide a quantitative description of its basic features. Theoretical results and experimental measurements are compared.

PACS numbers: 43.20.Fn, 43.35.Pt

I. INTRODUCTION

An analytical formulation to treat the reflection of a bounded ultrasonic beam at a liquid-solid interface was first established by Schoch.[1] That theory predicts a lateral displacement of the reflected beam for all total reflection angles. This simplified model fails to account for various experimentally observed phenomena at the Rayleigh critical angle. Making use of the existence of a pole-zero pair in the reflection coefficient at the Rayleigh critical angle, Bertoni and Tamir[2] describe an analytical approximation model that is able to explain all important features of the nonspecular reflectivity at the Rayleigh angle. Their approximation method for a liquid-solid interface has been subsequently extended to a study of reflectivity from a solid plate immersed in a liquid,[3] the diffraction effect observed away from the interface,[4] and the influence of attenuation[5] in the solid medium. Recently, the same Rayleigh-angle nonspecular reflectivity problem was investigated by means of a numerical integration method which produces results consistent with those of Bertoni and Tamir,[2] but also allows one to calculate changes in the profiles of the reflected beam for angles of incidence near the Rayleigh critical angle.[6]

While nonspecular reflectivity near the Rayleigh critical angle has been studied extensively, little is known about the possible nonspecularly reflected phenomena for bounded beams incident at or near the longitudinal and shear critical angles. Experimental evidence indicating the existence of nonspecular reflectivity similar to that at the Rayleigh angle was reported by Neubauer[7] for Mallory 1000 at the shear critical angle and for Pyrex glass at the longitudinal critical angle.

This paper is intended to determine the reflected beam profile of a bounded sound beam incident at and near the longitudinal critical angle of a liquid-solid interface.

II. EFFECT OF ABSORPTION ON PLANE WAVE REFLECTION COEFFICIENT

A convenient form of the infinite plane wave amplitude reflection coefficient R for a liquid-solid interface is given[8] by

$$R(k_x) = \frac{(k_s^2 - 2k_x^2)^2 + 4k_x^2\kappa_s\kappa_d - \rho k_s^4\kappa_d/\kappa}{(k_s^2 - 2k_x^2)^2 + 4k_x^2\kappa_s\kappa_d + \rho k_s^4\kappa_d/\kappa}, \quad (1)$$

where

ρ = liquid density/solid density,

$k = \omega/v$,

$k_d = \omega/v_d$,

$k_s = \omega/v_s$,

$k_x = k \sin\theta_i$,

$\kappa = (k^2 - k_x^2)^{1/2}$,

$\kappa_d = (k_d^2 - k_x^2)^{1/2}$,

$\kappa_s = (k_s^2 - k_x^2)^{1/2}$,

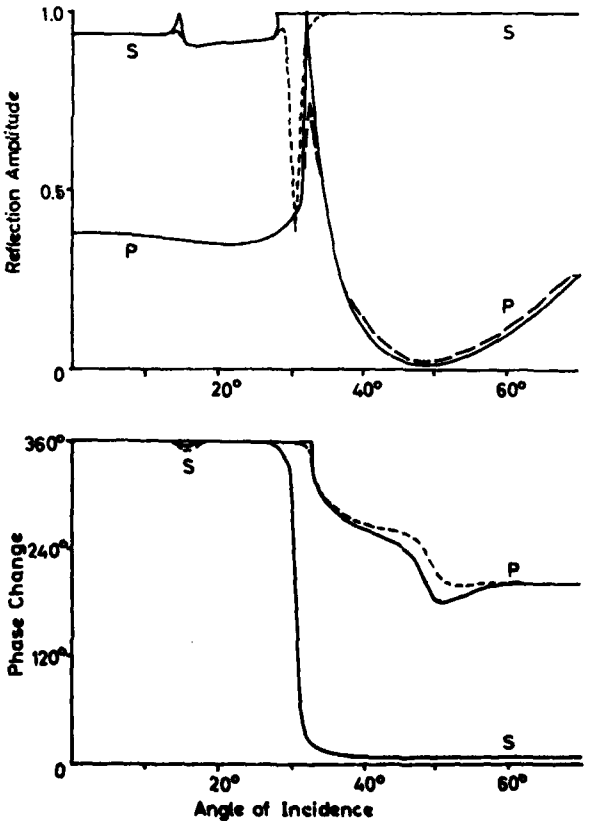

FIG. 1. Magnitude and phase of the reflection coefficient. The absorptive cases are denoted by dashed curves and the lossless cases by solid curves. *P* denotes a water-Plexiglas interface for a frequency of 2 MHz and *S* denotes a water-stainless steel interface for 15 MHz.

 0021-8979/79/127948-04$01.10

TABLE I. Sound velocities and density ratios.

Materials	v_d (m/sec)	v_s (m/sec)	ρ
Stainless steel	5840	3130	0.126
Plexiglas	2740	1350	0.84
Water	1480	...	1

where ω is the angular frequency, θ_i is the incident angle, v is the sound velocity in the liquid, and v_d and v_s are the velocities of the longitudinal and shear waves in the solid, respectively. The x direction is along the interface, and the incidence is from the liquid half-space.

It is known that the behavior of $R(k_x)$ is critically dependent on the attenuation constants of the media, especially at the Rayleigh critical angle, where the so-called "least-reflection frequency" is normally observed for many solids.[9] Near the longitudinal and shear critical angles, attenuation only slightly affects the magnitude and the phase of $R(k_x)$. However, it should be noted that inclusion of attenuation into the expression for $R(k_x)$ does smooth out the discontinuous behavior of the first derivatives of the magnitude and the phase of $R(k_x)$. In the complex plane of k_x, inclusion of attenuation results in the property that the branch points $\pm k$, $\pm k_d$, and $\pm k_s$ of $R(k_x)$ and their corresponding branch cuts are then located off the real axis. This shift of position of the branch points makes a numerical integration method possible.

The effects due to attenuation in materials can be incorporated into $R(k_x)$ by introducing the complex wave numbers k, k_d, and k_s as defined below. Denoting a as attenuation per wavelength for the sound wave in the liquid, and a_d and a_s for the longitudinal and shear waves in the solid, the complex wave numbers can be written as

$$k = (\omega/v)\,(1 + ia/2\pi)\,,$$
$$k_d = (\omega/v_d)\,(1 + ia_d/2\pi)\,, \qquad (2)$$
$$k_s = (\omega/v_s)\,(1 + ia_s/2\pi)\,.$$

To illustrate the influence of attenuation, the magnitude and the phase of $R(k_x)$ are plotted as functions of the angle of incidence for water-stainless steel and water-Plexiglas interfaces with and without attenuation (Fig. 1). The parameter values used to produce these curves and all subsequent figures are given in Tables I and II.

Figure 1 shows that the curves for stainless steel are typical of many other solid/liquid combinations as previously reported,[9] while those for Plexiglas exhibit a remarkably different pattern, expecially near the longitudinal critical angle ($\theta_L = 32.70°$).

TABLE II. Attenuation data.

Materials	Frequencies (MHz)	a_d	a_s
Plexiglas	1	0.0104	0.0107
	2	0.0271	0.0496
	6	0.1027	0.5670
Stainless steel	15	0.0108	0.0314
Water	all	0.00026	...

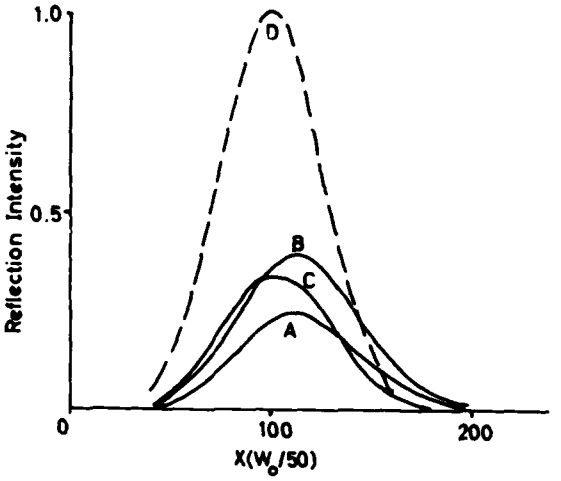

FIG. 2. Reflected beam profiles for a bounded beam of 0.75-in. width incident at θ_L onto a water-Plexiglas interface. The dashed line represents the incident beam, the solid lines represent the reflected beam profile for (A) 1 MHz, (B) 2 MHz, (C) 6 MHz.

III. NONSPECULAR REFLECTION OF A BOUNDED BEAM AT LONGITUDINAL CRITICAL ANGLE

Since the strongly varying behavior of $R(k_x)$ near the Rayleigh angle leads to pronounced nonspecular reflectivity while the effect is insignificant where $R(k_x)$ does not possess this characteristic,[6] one may expect, on the basis of the results shown in Fig. 1, that Plexiglas may also show nonspecular reflection for incidence near the longitudinal critical angle.

Using the method of representing a bounded sound beam by a Fourier integral in k space,[2] a numerical integration algorithm is developed on the basis of Simpson's Rule to calculate the reflected beam profile of a Gaussian incident beam. The advantage of this method is the possibility of investigating nonspecular reflectivity for any angle of incidence and for non-Gaussian incident beam profiles as well as the Gaussian one. The method has been used[6] to study the nonspecular reflection phenomena near the Rayleigh angle. Here it will be used to examine reflectivity in the angular range about the longitudinal critical angle.

It was shown by Bertoni and Tamir[2] that the amplitude field of a bounded beam reflected from a liquid-solid interface can be described by an integral, which, after slight modifications, normalization, and several changes of variables to facilitate the integration process, is given by

$$U_r(X) = (2\pi)^{-1/2} \int_{A_i - W_k}^{A_i + W_k} R(A_x) V(A_x) E(A_x, X)\, dA_x\,, \quad (3)$$

where

$$R(A_x) = \frac{(2A_x^2 - A_s^2)^2 + 4B_d B_s A_x^2 - \rho A_s^4 B_d/B}{(2A_x^2 - A_s^2)^2 + 4B_d B_s A_x^2 + \rho A_s^4 B_d/B}\,,$$
$$V(A_x) = C \exp\left[-(\tfrac{1}{2}C)^2\,(A_x - A_i)^2\right],$$

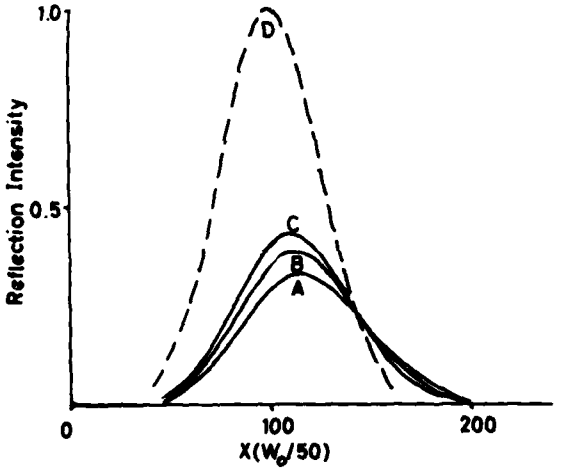

FIG. 3. Reflected beam profiles for a bounded beam of frequency 2 MHz incident at θ_i onto a water-Plexiglas boundary. The beam width is (A) 0.5 in., (B) 0.75 in., (C) 1.0 in. The dashed line represents the incident beam.

$$E(A_x, X) = \exp(iCA_xX),$$

where

$$A = 1 + ia/2\pi,$$

$$A_d = (v/v_d)(1 + ia_d/2\pi),$$

$$A_s = (v/v_s)(1 + ia_s/2\pi),$$

$$B = (A^2 - A_x^2)^{1/2},$$

$$B_d = (A_d^2 - A_x^2)^{1/2},$$

$$B_s = (A_s^2 - A_x^2)^{1/2},$$

$$A_i = \sin\theta_i,$$

$$X = x/w_0,$$

$$C = \omega w_p/v,$$

$$V_k = \pi/C,$$

with x being the coordinate along the interface, θ_i the incident angle, and $2w_0$ the beam width projected onto the interface.

As expected from observing the behavior of $R(k_x)$ for incidence near θ_L, the calculated reflected beam profiles for the case of water-stainless steel only show a small beam displacement of about 2% of $2w_0$ which is normally not observable. In contrast, for the case of water-Plexiglas, the displacement of the intensity peak in the reflected beam becomes much greater and can be observed experimentally. This characteristic of nonspecular reflection near θ_L is not only a strong function of the material properties, but also of the sound frequency, hence of a_d and a_s, the beam width, and the incident angle.

In Fig. 2 a set of beam profiles are plotted for different frequencies while keeping the same incident beam width. The beam displacement is found to be larger for lower frequencies. Figure 3 shows another set of reflected beam profiles for a sound frequency of 2 MHz with the beam width 0.5, 0.75, and 1.0 in. . The calculations point to the fact that as the beam width is decreased, the beam displacement becomes larger but the peak intensity is reduced.

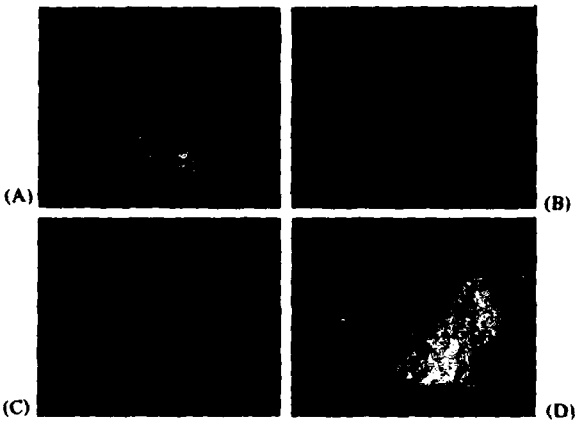

FIG. 4. Schlieren photographs showing beam displacement and changes in sound intensity near θ_L. The incident angle is (A) $\theta_L - 2°$, (B) $\theta_L - 1°$, (C) θ_L, (D) $\theta_L + 1°$.

IV. VARIATION OF BEAM PROFILE AS A FUNCTION OF ANGLE OF INCIDENCE NEAR θ_L

Reflected beam profiles change as a function of the angle of incidence. Their variation can be characterized by changes in the beam displacement and the intensity peak, which are only substantial near the longitudinal critical angle for a water-Plexiglas interface. The numerical integration method is now used to determine the reflection profiles of a beam of 2-MHz frequency and 0.75-in. width when the angle of incidence is varied by steps of 0.5°. The same phenomenon is also monitored by using the Schlieren visualization technique.

Figure 4 consists of a series of Schlieren photographs showing the gradual change in profiles of the beam reflected at angles first smaller than θ_L and becoming larger until exceeding θ_L. A sharp increase in the beam displacement and the reflected intensity can be detected for an incident

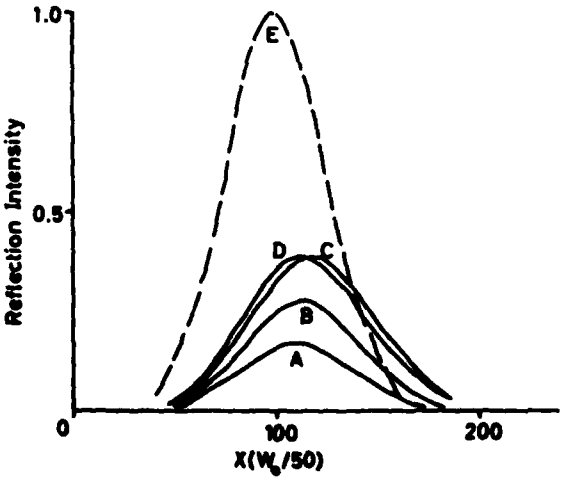

FIG. 5. Reflected beam profiles for a bounded beam of frequency 2 MHz and beam width of 0.75 in. incident at a water-Plexiglas interface at (A) $\theta_L + 3°$, (B) $\theta_L + 2°$, (C) $\theta_L + 1°$, (D) θ_L. The dashed line represents the incident beam.

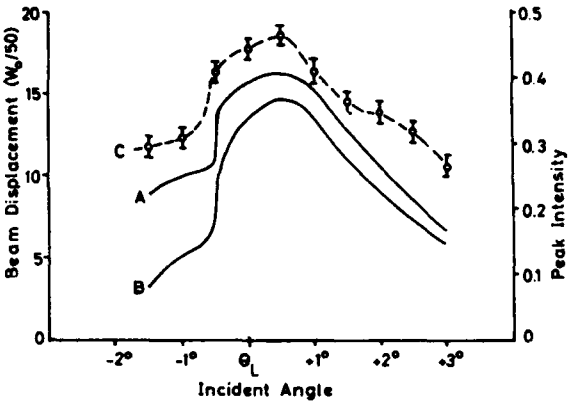

FIG. 6. Peak intensity and displacement of a bounded beam between $\theta_L - 2°$ and $\theta_L + 3°$ for a water-Plexiglas interface, beam width of 0.75 in., and frequency of 2 MHz. Curve (A) shows the theoretical peak intensity variation. The theoretical and experimentally measured beam displacements are denoted by curves (B) and (C), respectively.

angle slightly less than θ_L. A number of these profiles are theoretically determined and shown in Fig. 5 for $\theta_L < \theta_i < \theta_L + 3°$.

In order to establish the exact relationship between the beam displacement and θ_i, calculations are done for smaller increments of the incident angle. The results plotted in Fig. 6 indicate the existence of such a sharp increase simultaneously in both beam displacement and reflection intensity. Comparison of Figs. 6 and 4 shows qualitative agreement between theory and experiment. Measurements of the beam displacement from the Schlieren photographs are also shown in Fig. 6. Both calculated and experimental curves exhibit the same general variation pattern for the beam displacement with respect to the incident angle. The uncertainty in the absolute values of the beam displacement is due to the fact that small differences between the values of v_d, v_s, ρ, a_d, and a_s listed in Tables I and II and those which apply to a particular Plexiglas sample will cause the calculated displacement to differ from the observed one. The greatest uncertainty for this calculation lies in the values of the shear-wave velocity and absorption for Plexiglas. These values are not known to a high degree of accuracy.

V. CONCLUSION

The above calculated results obtained by a numerical integration method and experimental measurements establish the fact that there exists nonspecular reflectivity near the longitudinal critical angle for a liquid-solid interface. This phenomenon is found to be significant only for certain liquid-solid combinations, one of which is water-Plexiglas. For incidence near the longitudinal critical angle, nonspecular reflectivity is most prominently characterized by a substantial beam displacement which varies with the incident angle, the beam width, and the frequency-dependent attenuation in materials. In general, the numerical integration method is shown to be applicable at a range of incident angles, where no successful analytical formulation had been available.

ACKNOWLEDGMENT

This work was supported by the Office of Naval Research, U.S. Navy.

[1]A. Schoch, Ergeb, Exakt. Naturw. **23**, 127 (1950).
[2]H.L. Bertoni and T. Tamir, J. Appl. Phys. **2**, 157 (1973).
[3]L.E. Pitts, T.J. Plona, and W.G. Mayer, IEEE Trans. Sonics Ultrason. SU-**24**, 101 (1977).
[4]M.A. Breazeale, L. Adler, and G.W. Scott, J. Appl. Phys. **48**, 530 (1977).
[5]H.L. Bertoni and Y.L. Hou, Proc. 10th Symp. NDE **10**, 136 (1975).
[6]T.D.K. Ngoc, Ph.D. thesis, Georgetown University, 1979.
[7]W.G. Neubauer, J. Appl. Phys. **44**, 48 (1973).
[8]L.E. Pitts, Ph.D. thesis, Georgetown University, 1975.
[9]F.L. Becker and R.L. Richardson, J. Acoust. Soc. Am. **51**, 1609 (1972).

Numerical integration method for reflected beam profiles near Rayleigh angle

Tran D. K. Ngoc and Walter G. Mayer

Physics Department, Georgetown University, Washington, D.C. 20057
(Received 16 July 1979; accepted for publication 31 December 1979)

A numerical integration method is devoloped to calculate the intensity profile of an ultrasonic beam reflected from a liquid–solid interface. This numerical treatment is used to calculate nonspecular reflectivity at a range of angles of incidence near and at the Rayleigh angle. Calculations for a water–stainless steel interface are compared to a known approximate analysis for various beamwidths and frequencies. The theoretical predictions of the reflected beam profile near the Rayleigh angle of incidence are compared to experimental results.

PACS numbers: 43.20.Fn, 43.20.Rz

INTRODUCTION

Nonspecular reflection effects for ultrasonic waves were originally predicted and experimentally verified by Schoch[1] and later by Neubauer[2] and Breazeale *et al.*[3] for bounded beams incident on a liquid–solid interface. The simple model presented by Schoch does not account completely for different experimentally observed phenomena at Rayleigh critical angle, such as the point of intensity minimum and the trailing field. These discrepancies have been eliminated by Bertoni and Tamir[4] who use a complex Laurent series expansion to simplify the mathematically complicated expression of reflection coefficient in terms of its complex pole and zero. Bertoni and Tamir's approximation gives excellent results at the Rayleigh critical angle which is associated with the complex pole and zero.

Attenuation in the media involved, when included in these analyses, further complicates the physical problem. Becker and Richardson[5] pointed out the different behavior of the reflectcn coefficient with absorption being taken into account. In such cases, total reflection is not expected at any angle of incidence and the reflection amplitude and phase are shown to deviate significantly from the lossless case.

Recently, Bertoni and Hou[6] have modified their formulation to incorporate attenuation into their theoretical investigation of nonspecular reflectivity. Pitts *et al.*[7] have extended Bertoni and Tamir's results to a more complicated case of the liquid–solid–liquid plate structure. Breazeale *et al.*[8] used Bertoni and Tamir's analysis to investigate the reflected beam profiles observed at large distances from the liquid–solid interface.

Bertoni and Tamir's approximation, although giving excellent results, has some limitations. It is not readily applicable to those critical angles other than the Rayleigh critical angle and presents considerable analytical problems when extended to non-Gaussian beam profiles.

In the following, the reflected profile is determined by numerically integrating the Fourier integral describing the reflected beam amplitude, taking into account the attenuation in the materials involved. The reflected profiles are calculated and compared to known results when one varies one of the physical parameters, namely, the beamwidth, the sound frequency, and the incident angle.

I. MATHEMATICAL REPRESENTATION OF BOUNDED BEAMS

In Fig. 1, a Gaussian sound beam with a beamwidth $2w$ is shown to be incident at an angle θ_i from a liquid onto a solid medium. The amplitude field of a sound beam with finite lateral dimensions can be expressed as a sum of infinte plane waves via a Fourier transform pair.[4] An incident bounded beam can then be represented by

$$U_{\rm inc}(x, z) = (2\pi)^{-1}\int_{-\infty}^{\infty} V(k_x)\exp[i(k_x x + k_z z)]\,dk_x \qquad (1)$$

and

$$V(k_x) = \int_{-\infty}^{\infty} U_{\rm inc}(x, 0)\exp(-i k_x x)\,dx, \qquad (2)$$

where the time dependence $\exp(-i\omega t)$ has been suppressed, k_x is the x component of the wave vector, $V(k_x)$ is the Fourier transform of the incident beam amplitude at $z = 0$, and k_z is defined by

$$k_z = (k^2 - k_x^2)^{1/2},$$

with k being the propagation wavenumber of the sound beam in the liquid.

The width of the area projected by such an incident beam onto the interface is $2w_0$, which is given by

$$w_0 = w\sec\theta_i .$$

Thus for well-defined beams, the range of integration in Eqs. (1) and (2) effectively is

$$(k_i - \pi/w_0) \leq k_x \leq (k_i + \pi/w_0) \qquad (3)$$

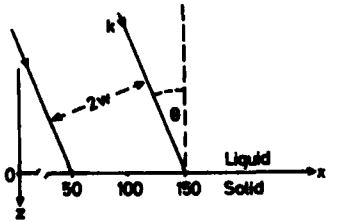

FIG. 1. A bounded sound beam incident onto the plane interface with a solid. The scale of the x axis is chosen arbitrarily for the center of the incident beam to be at 100.

 0001-4966/80/041149-04$00.80

and

$$-w_0 \le x \le w_0, \tag{4}$$

where

$$k_t = k \sin\theta_t .$$

The Fourier integral for the incident beam $U_{inc}(x, z)$ can be interpreted as being a superposition of an infinite number of incident plane waves with different amplitudes $V(k_x)$, all of the same wavelength but incident at different angles within a narrow angular range about θ_t. Extending this interpretation, one can represent the reflected beam profile by integrating over individual reflected plane waves which are now affected by the plane wave reflection coefficient $R(k_x)$ as

$$U_R(x, z) = (2\pi)^{-1} \int_{-\infty}^{\infty} R(k_x) V(k_x) \exp[i(k_x x + k_z z)]\, dk_x . \tag{5}$$

At the interface $z = 0$ this expression reduces to

$$U_R(x, 0) = (2\pi)^{-1} \int_{-\infty}^{\infty} R(k_x) V(k_x) \exp(ik_x x)\, dk_x , \tag{6}$$

with $R(k_x)$ being given by[9]

$$R(k_x) = \frac{(k_s^2 - 2k_x^2)^2 + 4k_x^2 \kappa_s \kappa_d - \rho k_s^4 \kappa_d/\kappa}{(k_s^2 - 2k_x^2)^2 + 4k_x^2 \kappa_s \kappa_d + \rho k_s^4 \kappa_d/\kappa}, \tag{7}$$

where

ρ = liquid density/solid density,

$k = \omega/v$, $k_d = \omega/v_d$, $k_s = \omega/v_s$,

$\kappa = (k^2 - k_x^2)^{1/2}$,

$\kappa_d = (k_d^2 - k_x^2)^{1/2}$, $\kappa_s = (k_s^2 - k_x^2)^{1/2}$,

where v is the sound velocity in the liquid and v_d and v_s the velocities of the longitudinal and shear waves in the solid, respectively.

II. AN APPROXIMATE ANALYTICAL SOLUTION TO THE REFLECTED BEAM INTEGRAL

Expanding $R(k_x)$ in a Laurent series, Bertoni and Tamir were able to derive an approximate form for $R(k_x)$ which yields the reflected beam profile expressed by Eq. (6) for a Gaussian beam incident at the Rayleigh critical angle. With the incident Gaussian beam being normalized to unity, the incident and reflected beam intensity profiles can be written as[4]

$$|U_{inc}(x, 0)|^2 = \exp[-2(x/w_0)^2] \tag{8}$$

and

$$|U_R(x, 0)|^2 = |R_1 + R_2 R_3^2|\, |U_{inc}(x, 0)|^2 , \tag{9}$$

where

$$R_1 = (\mathrm{Re}\, k_p - k_0)/(\mathrm{Re}\, k_p - k_p),$$

$$R_2 = (k_p - k_0)/(k_p - \mathrm{Re}\, k_p),$$

$$R_3 = 1 - [(\pi^{1/2} w_0 \,\mathrm{Im}\, k_p/2) \exp(\gamma^2)\, \mathrm{erfc}(\gamma)],$$

where

k_p = Pole of $R(k_x)$,

k_0 = Zero of $R(k_x)$,

$\gamma = (w_0 \,\mathrm{Im}\, k_p/2) - (x/w_0)$.

Briefly, the Bertoni and Tamir's formulation requires that the pole and zero locations be identified before the reflected profile can be determined by Eqs. (8) and (9).

III. INCORPORATION OF ATTENUATION IN THE MEDIA

Effects of attenuation in materials can be incorporated in the wave vectors k, k_d, and k_s. Denoting a, a_d, and a_s as attenuation per wavelength for the sound waves in liquid, the longitudinal waves, and the shear waves in the solid, respectively, one can write the wave vectors for the absorptive media as

$$\begin{aligned} k &= (\omega/v)(1 + ia/2\pi), \\ k_d &= (\omega/v_d)(1 + ia_d/2\pi), \\ k_s &= (\omega/v_s)(1 + ia_s/2\pi). \end{aligned} \tag{10}$$

Inclusion of attenuation moves the branch points k, k_d, and k_s off the real axis. Analytically, introduction of attenuation into the terms contained in the reflection coefficient [Eq. (7)] makes $R(k_x)$ differentiable even at the longitudinal and shear critical angles. For the lossless case, the reflection coefficient is frequency-independent. In practice, this is not the case since one usually observed in experiments different profiles for different frequencies.

Bertoni and Hou[6] show that the values of k_p and k_0 will change with the frequency-dependent values of a_d and a_s, making the simplifying assumption that $a_d = a_s$ and that the absorption in the liquid medium can be neglected for a water–stainless steel interface. Under these simplifying conditions the value of k in Eq. (10) reduces to a real quantity, and the imaginary parts are the same for both k_d and k_s. However, if one uses distinct values for a_d and a_s, and includes attenuation in the liquid, the loci of k_p and k_0 are different from those obtained under these simplifying assumptions.

The results of such calculations for a water–stainless steel interface are shown in Fig. 2(a). The values of the longitudinal and shear wave absorption coefficients used are those given by Fitch[10] ($a_d = 0.00017$, $a_s = 0.00024$) and the value of the attenuation in water was

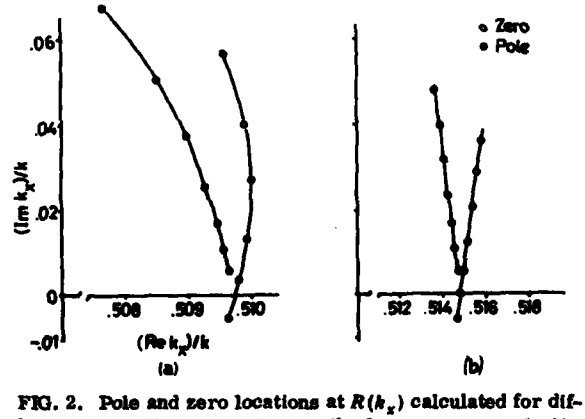

FIG. 2. Pole and zero locations at $R(k_x)$ calculated for different attenuation parameters in the frequency range 1–40 MHz for water–stainless steel interface when (a) $a_d = a_s$ and $a \neq 0$ (b) $a_d = a_s$ and $a = 0$.

assumed to be $a = 0.00026$. Figure 2(b), which is taken in part from Bertoni and Hou,[6] is reproduced for comparison. The results shown in Fig. 2(b) are based on the assumption that $a_d = a_s$ and that a is negligible. One notes that the loci of the poles and zeros in Fig. 2(a) no longer lie on a straight line. The values of $\mathrm{Re}(k_x)/\mathrm{Re}(k)$ are of no particular importance for the present discussion since they depend only on the assumed value of the sound velocity in water.

IV. BEAM PROFILES CALCULATED BY NUMERICAL INTEGRATION

In the Bertoni and Tamir's derivation, it is important to note that one must identify the Rayleigh pole and zero and that the reflection coefficient is approximated in the following form:

$$R(k_x) = (k_x - k_0)/(k_x - k_p). \tag{11}$$

It is shown[6] that Eq. (11) is only sufficiently accurate when the incident angle is at the Rayleigh critical angle. Away from the Rayleigh angle, the accuracy of Eq. (11) is reduced rapidly. It is realized that the reflected profile expressed by Eq. (6) can also be calculated by numerical integration. Since the exact form of the reflection coefficient is to be used, such a numerical approach can provide an accurate profile even away from the Rayleigh critical angle without a prior knowledge of the pole-zero location.

After normalization with respect to an incident beam with a Gaussian profile and making use of the effective integral limits given by Eqs. (3) and (4), Eq. (6) can be written as

$$U_r(X) = (2\pi)^{-1/2} \int_{A_i - W_h}^{A_i + W_h} R(A_x) V(A_x) E(X, A_x)\, dA_x, \tag{12}$$

where

$$R(A_x) = \frac{(2A_x^2 - A_s^2)^2 + 4B_dB_sA_x^2 - A_s^4B_d/B}{(2A_x^2 - A_s^2)^2 + 4B_dB_sA_x^2 + A_s^4B_d/B},$$

$$V(A_x) = C\exp[-(C/2)^2(A_x - A_i)^2],$$

$$E(X, A_x) = \exp(iCA_xX),$$

where the new dimensionless variables are defined as follows:

$$A = 1 + ia/2\pi, \quad A_d = (v/v_d)(1 + ia_d/2\pi),$$

$$A_s = (v/v_s)(1 + ia_s/2\pi), \quad B = (A^2 - A_x^2)^{1/2},$$

$$B_d = (A_d^2 - A_x^2)^{1/2}, \quad B_s = (A_s^2 - A_x^2)^{1/2},$$

$$A_i = \sin\theta_i, \quad X = x/w_0, \quad C = \omega w_0/v, \quad W_h = \pi/C.$$

The reflected profiles which are shown in the next section are numerically determined according to Eq. (12).

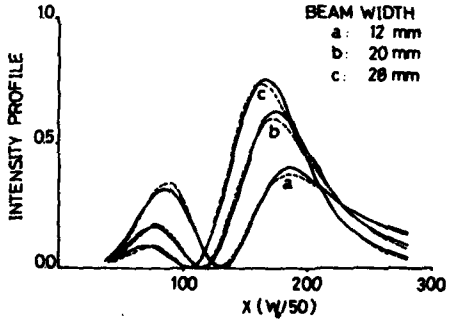

FIG. 3. Reflected beam profiles at 2 MHz for various beamwidths using both Bertoni and Tamir's analysis and numerical integration with $\Theta_i = \Theta_r$ for a water–stainless steel interface. Solid curves are those calculated by numerical method.

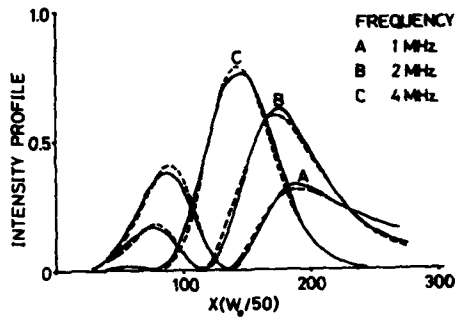

FIG. 4. Reflected beam profiles for beamwidth equal to 20 mm at various frequencies using both Bertoni and Tamir's analysis and numerical integration with $\Theta_i = \Theta_r$ for a water–stainless steel interface. Solid curves are those calculated by numerical integration.

V. CALCULATED AND EXPERIMENTAL RESULTS

In this section, the reflected profile is calculated by two approaches for different sets of physical parameters. First, the frequency is kept constant while the beamwidth is being changed. Then, the beamwidth is held constant as one varies the sound frequency. In these two cases, the beam is incident at the Rayleigh angle and the values of k_p and k_0 substituted in the results derived by Bertoni and Tamir are obtained from the attenuation data which are entered into the numerical integration approach. This was done to eliminate the possible discrepancy which may arise due to different data used for attenuation. Finally, the profiles of the reflected beam is calculated when the incident angle is varied near the Rayleigh critical angle.

In Fig. 3, the reflected beam profile is plotted for different beamwidths at 2 MHz for a water–stainless

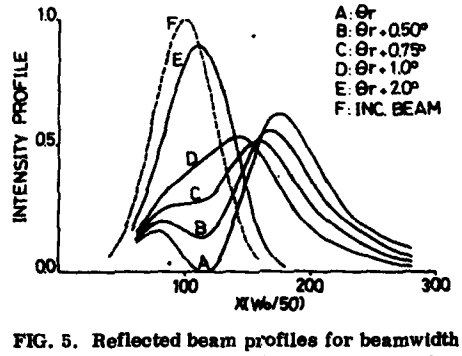

FIG. 5. Reflected beam profiles for beamwidth equal to 20 mm at 2 MHz using numerical integration when Θ_i is slightly varied from Θ_r for a water–stainless steel interface.

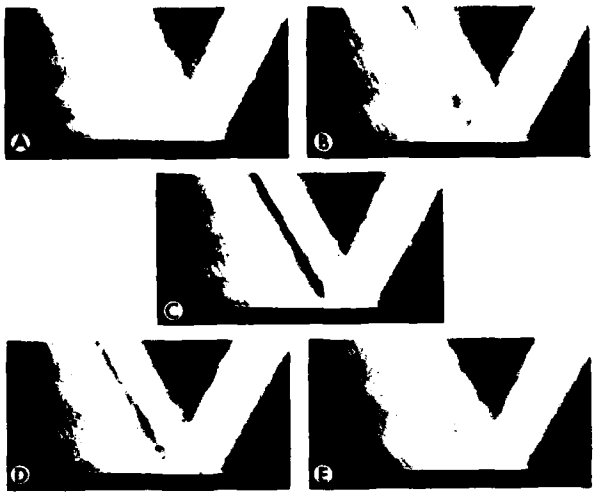

FIG. 6. Schlieren pictures of beam profiles at five different angles of incidence about Θ_r for a water–stainless steel interface. *A*: $\Theta_i = \Theta_r - 1°$; B: $\Theta_i = \Theta_r - 0.5°$; C: $\Theta_i = \Theta_r$; D: $\Theta_i = \Theta_r + 0.5°$; E: $\Theta_i = \Theta_r + 1.0°$.

steel interface. Results obtained by both methods, Bertoni and Tamir's analysis and the numerical integration, are presented in this figure. Also for the water–stainless steel interface, the reflected profiles are plotted in Fig. 4 for various frequencies while the beamwidth remains unchanged. Again, both results are shown in the same figure. It is seen that Bertoni and Tamir's analysis, although using an approximate form for $R(k_x)$, agrees very well with an almost exact calculation.

Figure 5 shows the results for a 2-MHz beam incident on a water–stainless steel interface when the incident angle is varied from the Rayleigh critical angle. A gradual change in the beam profile is noticeable, in particular, the slow increase in intensity in the "null intensity" as the specularly and nonspecularly reflected sections of the beam merge into one with lessening beam displacement.

The same gradual change is observed experimentally. Figure 6 consists of a series of Schlieren photographs of the incident and reflected beams for a water–stainless steel interface. The beamwidth and the sound frequency used were 19 mm and 1.96 MHz. The incident angle was varied by steps of 0.25°.

It should be noted that the profile of the ultrasonic beam used was nearly Gaussian so that agreement between theory and experiment exists qualitatively. It should also be noted that the same type of agreement exists between experiment and the predictions of the present theory for reflection at angles greater or smaller than the Rayleigh angle by up to 2°. This range is sufficiently large so that differences between the approximate formulation and the numerical integration method become noticeable.

VI. CONCLUSION

It is shown that a numerical integration method can be used to determine accurately the reflected beam profile for a liquid–solid interface. The method is not restricted to calculations at the Rayleigh angle but can be extended to other angles of incidence,[11] where the analytical analysis[4] cannot be applied. The results obtained by the two methods do agree at and very near the Rayleigh critical angle. Schlieren photographs of the reflected beam at and near the Rayleigh critical angle show qualitative agreement between the results of the numerical integration method and experiments.

ACKNOWLEDGMENT

This work was supported by the Office of Naval Research, U.S. Navy.

[1]A. Schoch, "Schallreflexion, Schallbrechung and Schallbeugung," Ergeb. Exaktkn. Naturwiss. **23**, 127–234 (1950).
[2]W. G. Neubauer, "Ultrasonic Reflection of a Bounded Beam at Rayleigh and Critical Angles for a Plane Liquid–Solid Interface," J. Appl. Phys. **44**, 48–55 (1973).
[3]M. A. Breazeale, L. Adler, and J. H. Smith, "Energy Distribution of a Gaussian Ultrasonic Beam Relected from Liquid–Solid Interface," Sov. Phys.-Acoust. **21**, 1–5 (1975).
[4]H. L. Bertoni and T. Tamir, "Unified Theory of Rayleigh-Angle Phenomena for Acoustic Beams at Liquid–Solid Interface," Appl. Phys. **2**, 157–172 (1973).
[5]F. L. Becker and R. L. Richardson, "Influence of Material Properties on Rayleigh Critical-Angle Reflectivity," J. Acoust. Soc. Am. **51**, 1609–1617 (1972).
[6]H. L. Bertoni and Y. L. Hou, "Effects of Damping in a Solid on Acoustic Beams Reflected at the Rayleigh Critical Angle," Proc. 10th. Symp. NDE, San Antonio, TX 136–142 (1975).
[7]L. E. Pitts, T. J. Plona, and W. G. Mayer, "Theory of Non-Specular Reflection Effects for an Ultrasonic Beam Incident on a Solid Plate in a Liquid," IEEE Trans. Sonics Ultrason. **24**, 101–109 (1977).
[8]M. A. Breazeale, L. Adler, and G. W. Scott, "Interaction of Ultrasonic Waves Incident at the Rayleigh Angle onto a Liquid–Solid Interface," J. Appl. Phys. **48**, 530–537 (1977).
[9]L. E. Pitts, "A Unified Theoretical Description of Ultrasonic Beam Reflections from a Solid Plate in a Liquid," Ph.D. thesis, Physics Department, Georgetown University, Washington DC (1975).
[10]C. E. Fitch, Jr., "New Methods for Measuring Ultrasonic Attenuation," J. Acoust. Soc. Am. **40**, 989–997 (1966).
[11]T. D. K. Ngoc and W. G. Mayer, "Ultrasonic Non-Specular Reflectivity near Longitudinal Critical Angle," J. Appl. Phys. **50**, 7948–7951 (1979).

NONSPECULAR TRANSMISSION EFFECTS FOR ULTRASONIC BEAMS INCIDENT ON A SOLID PLATE IN A LIQUID

K.W. Ng, T.D.K. Ngoc
J.A. McClure, W.G. Mayer
Department of Physics
Georgetown University
Washington, DC 20057

The nonspecular phenomena are investigated theoretically for an ultrasonic beam transmitted through a solid plate immersed in a liquid. The analytical method used by Bertoni and Tamir [3] to describe the nonspecular profile of a beam reflected from a liquid-solid interface is extended to the problem under consideration, taking into account all existing poles. To solve the integral representing the transmitted beam, the amplitude-plane wave transmission coefficient is replaced by a simpler approximate form. The transmitted beam profile is then calculated from both single-pole and multiple-pole formulations.

I. Introduction

Since the work of Goos and Hanchen in 1947, it has been known that light waves are not always reflected geometrically but may be shifted in the specular plane at some angles of incidence[1]. Similar displacements have been observed with sound beams as well as other non-specular phenomena, namely, a null strip in the reflected beam, and a trailing sound field which follows the primary reflection and decreases in intensity as it moves down the interface. In the early investigations of these effects, Schoch [2] proposed a simple theory which explained the displacement of the sound beam but failed to account for other non-specular features.

More recently Bertoni and Tamir [3] have proposed a theory which successfully accounts for all observed non-specular phenomena in reflection from a liquid-solid (L/S) interface. These authors emphasize the use of complex poles of the plane wave reflection coefficient in determining both an approximate mathematical form of the coefficient itself and in finding an accurate description of the reflected sound intensity profile. Pitts [4] has extended the approach of Bertoni and Tamir to the study of the reflection of a sound beam from a liquid-solid-liquid (L/S/L) system.

Experimental observation has shown that non-specular phenomena occur in the transmitted beam as well. In this investigation we will take the general theoretical approach used by Bertoni and Tamir and by Pitts and extend it to the problem of the transmission of a bounded acoustic beam through an L/S/L system [5].

II. Theory of the Reflection and Transmission of a Bounded Beam by a Solid Plate

Consider a bounded acoustic beam of width 2W incident at angle θ_i on a

solid plate of width d immersed in a liquid. The coordinate system is as shown in Fig. 1 where the incident, reflected and transmitted beams are depicted. The plate's incident surface is taken to form the xy plane. The sound field is assumed to be uniform in the direction perpendicular to the plane of incidence and, therefore, has no spatial y dependence. Using Fourier integrals, the particle displacement amplitude $U_{inc}(x,z)$ associated with the incident sound field can be expressed as a sum of infinite plane waves,

$$U_{inc}(x,z) = \frac{1}{2\pi}\int_{-\infty}^{\infty} V(R_x)\exp\left[i(xR_x + zR_z)\right] dR_x . \tag{1}$$

Here k_x is the projection of the incident wave vector on the x-axis, $k_x = k\sin\theta$, with θ the angle of incidence of the plane wave, and $k_z^2 = k^2 - k_x^2$. The amplitude $V(k_x)$ of the plane wave components of the incident beam can be obtained by Fourier inversion from the initial beam on the z = 0 or incident surface of the plate,

$$V(R_x) = \int_{-\infty}^{\infty} U_{inc}(x,0)\exp\left[-ixR_x\right] dx . \tag{2}$$

The Fourier integral of the incident beam can be interpreted as being composed of an infinite number of plane waves, all of the same wavelength but at different incident angles θ with respect to the normal to the surface. If this interpretation is extended to the sound fields reflected and transmitted by the plate, they too can be expressed as a sum over individual plane waves by using the reflection and transmission coefficients, $R(k_x)$ and $T(k_x)$ for the L/S/L system,

$$\begin{aligned} U_R(x,z) &= \frac{1}{2\pi}\int_{-\infty}^{\infty} R(R_x)V(R_x)\exp\left[i(xR_x + zR_z)\right] dR_x , \\ U_T(x,z) &= \frac{1}{2\pi}\int_{-\infty}^{\infty} T(R_x)V(R_x)\exp\left[i(xR_x + zR_z)\right] dR_x . \end{aligned} \tag{3}$$

Any evaluation of the reflected and transmitted sound beams depends, among other things, on the amplitude distribution of the incident beam $\underset{\sim}{U}_{inc}(x,0)$. Most transducers produce roughly a Gaussian beam for which a reasonable approximation is

$$U_{inc}(x,z) \propto \exp\left[-\left(\xi/W\right)^2\right],$$

where W is the half beam width and ξ is a coordinate transverse to the beam propagation direction. A convenient form for the incident profile is

$$\underset{\sim}{U}_{inc}(x,0) = \exp\left[-\left(x/W_0\right)^2 + i\,x\,R_i\right], \tag{4}$$

where $W_0 = W \sec\theta_i$, $R_i = R \sin\theta_i$, and θ_i is the beam's incident angle as defined in Fig. 1. Combining (4) and (2) we get

$$V(R_x) = \sqrt{\pi}\, W_0 \exp\left[-\left(R_i - R_x\right)^2 \left(W_0/2\right)^2\right] \tag{5}$$

and for the reflected and transmitted sound field amplitudes at the appropriate surfaces

$$U_R(x,0) = \frac{W_0}{2\pi^{1/2}} \int_{-\infty}^{\infty} R(R_x) \exp\left\{-i\left(R_i - R_x\right)^2 \left(\frac{W_0}{2}\right)^2 + i\,x\,R_x\right\} d\,R_x, \tag{6}$$

$$U_T(x,d) = \frac{W_0}{2\pi^{1/2}} \int_{-\infty}^{\infty} T(R_x) \exp\left\{-i\left(R_i - R_x\right)^2 \left(\frac{W_0}{2}\right)^2 + i\left(x R_x - d R_2\right)\right\} d\,R_x. \tag{7}$$

An evaluation of these integrals and their comparison with experiment is a central problem in the study of the L/S/L system. The reflected beam has been thoroughly investigated by Pitts and others, and in this study we shall extend their treatment to the transmitted sound field.

III. The Amplitude Transmission Coefficient

The reflection and transmission coefficients which appear in (6) and (7) are obtained from the boundary conditions at the surfaces of the plate. A

straightforward but laborious calculation yields

$$R(R_x) = \frac{1}{f_s f_a}\left\{(R_s^2 - 2R_x^2)^4 + 16R_x^2 K_s^2 K_d^2 - \rho^2 R_s^8 K_d^2 K^{-2} + 8(R_s^2 - 2R_x^2)^2 R_x^2 K_s K_d \left(\frac{1 - \cos P \cos Q}{\sin P \sin Q}\right)\right\}, \tag{8}$$

$$T(R_x) = \frac{1}{f_s f_a}\left\{\frac{2i\rho R_s^4 K_d}{K}\right\}\left\{\frac{(R_s^2 - 2R_x^2)^2}{\sin P} + \frac{4R_x^2 K_s K_d}{\sin Q}\right\}, \tag{9}$$

where

$$f_s = (R_s^2 - 2R_x^2)^2\left\{\frac{1+\cos P}{\sin P}\right\} + 4R_x^2 K_s K_d\left\{\frac{1+\cos Q}{\sin Q}\right\} - i\frac{\rho R_s^4 K_d}{K}, \tag{10}$$

$$f_a = (R_s^2 - 2R_x^2)^2\left\{\frac{1-\cos P}{\sin P}\right\} + 4R_x^2 K_s K_d\left\{\frac{1-\cos Q}{\sin Q}\right\} + i\frac{\rho R_s^4 K_d}{K}, \tag{11}$$

where the following variables have been defined:

$$\begin{aligned}
\rho &= \rho_{liquid}/\rho_{solid}, \\
\kappa &= k\cos\theta = k(1-\sin^2\theta)^{1/2}, \\
\kappa_s &= k_s\cos\theta_s = k[(v/v_s)^2 - \sin^2\theta]^{1/2}, \\
\kappa_d &= k_d\cos\theta_d = k[(v/v_d)^2 - \sin^2\theta]^{1/2}, \\
P &= d\kappa_d, \\
Q &= d\kappa_s.
\end{aligned} \tag{12}$$

The coefficients (8) and (9) satisfy the relationship

$$|R(R_x)|^2 + |T(R_x)|^2 = 1 \tag{13}$$

appropriate to a lossless medium.

Because of the complicated dependence of $R(k_x)$ and $T(k_x)$ upon k_x, a direct evaluation of the profile integrals (6) and (7) is very difficult. Complex contour integration is a possibility but the presence of branch cuts in R and T poses difficulties if this approach is taken. Bertoni and Tamir in the case of reflection from the L/S interface, and later Pitts treating the L/S/L case, have addressed this problem by using an approximation for $R(k_x)$. The approximate reflection coefficient of the general form

$$R'(R_x) = \prod_{j=1}^{N} \left(\frac{R_x - z_j}{R_x - p_j} \right) \tag{14}$$

is constructed to have the same poles p_j, $p_j = \beta_j + i\alpha_j$, and the same zeros z_j as $R(k_x)$ but no other singularities. With $R(k_x)$ replaced by $R'(k_x)$, the integral (6) can be evaluated using the residue theorem.

We will follow that approach in this investigation and will construct approximations to the transmission coefficient. With these approximations the profile of the transmitted beam (7) will be evaluated and compared with experiment.

In a lossless medium the sum of reflected and incident energies must equal the incident energy, a condition expressed mathematically in Eq. (13). In the present investigation, where we shall try to use as much as possible the earlier results of Pitts, this equation will be the basis of our approximation procedure for T. Equation (13) states, among other things, that whenever $|R| = 0$, $|T| = 1$. Two very simple forms for T which have this property are

$$T'^{(N)}(R_x) = 1 - \prod_{j=1}^{N} \left(\frac{R_x - z_j}{R_x - p_j} \right) \tag{15}$$

and

$$T''^{(N)}(R_x) = \prod_{j=1}^{N} \left(1 - \frac{R_x - z_j}{R_x - p_j} \right), \tag{16}$$

in which z_j and p_j are respectively the zeroes and poles of $R(k_x)$ already introduced in connection with (14).

Each of these forms has its shortcomings. Let us denote the relative phase of T, T', and T'' by ψ, ψ', and ψ'', respectively. Then numerical evaluation of (15), (16), (9) and comparison show good agreement between $|T'|$ and $|T|$ but poor agreement between the phases ψ' and ψ. On the other hand, there is good agreement between ψ'' and ψ, but poor agreement between $|T''|$ and $|T|$.

IV. The Transmitted Beam Profile

In addition to the complexities of T, the integral (7) for the transmitted beam is complicated by the presence of the factor $\exp(dk_z)$ in the integrand. This factor does not appear in (6) because of the choice of the incident surface of the plate as the z = 0 surface. This problem can be addressed, however, by expanding k_z in a Taylor series about $\sin\theta$.

$$R_z = R\cos\theta - (R_x - R\sin\theta)\tan\theta + (R_x - R\sin\theta)^2/2R\cos^3\theta + \dots \quad (17)$$

All the terms are now in the proper form for the evaluation of the transmitted beam profile integral. Because of the complexity of the expressions, it is worthwhile defining an integral which plays an important role in the evaluation. It describes the profile of the incident beam at the z = d plane as if there were no solid plate present. Substitution of Eqs. (2) and (17) into (1) yields

$$U^{(0)}(x,d) = \frac{W}{2\pi^{\frac{1}{2}}\cos\theta}\int_{-\infty}^{\infty} \exp\left\{-(R_x - R\sin\theta)^2\left(\frac{W}{2\cos\theta}\right)^2\right\} \times \exp\left\{ixR_x + id\left[R\cos\theta - (R_x - R\sin\theta)\tan\theta + (R_x - R\sin\theta)^2/2R\cos^3\theta\right]\right\} dR_x . \quad (18)$$

After some manipulation this can be shown to become

$$U^{(0)}(x,z) = \frac{W}{W_T} \exp\left\{-\left(\frac{x_T}{W_T}\right)^2 + ikz_T\right\}, \tag{19}$$

in which the variables

$$\begin{aligned} x_T &= x\cos\theta - z\sin\theta, \\ z_T &= x\sin\theta + z\cos\theta, \\ w_T &= W[1 - (2iz/kW^2\cos\theta)]^{\frac{1}{2}}, \end{aligned} \tag{20}$$

have been introduced. Equations (19) and (20) not only describe the Gaussian incident beam in terms of a new set of coordinates, z_T parallel with and x_T transverse to the direction of incidence, but also explicitly express the beam spreading caused by the geometrical diffraction of a bounded beam.

The transmitted sound field amplitude (7) may now be evaluated for either of the approximations (15) or (16). The procedure is essentially the same for both, and we will present it here only for $T''(k_x)$. First noting that

$$T'' = \prod_{j=1}^{N}\left(1 - \frac{R_x - z_j}{R_x - \rho_j}\right) = \prod_{j=1}^{N}\left(-\frac{\rho_j - z_j}{R_x - \rho_j}\right)$$

then substituting into (7), we find

$$\begin{aligned} U_{T''}^{(N)}(x,z) &= \frac{W}{2\pi^{\frac{1}{2}}\cos\theta}\left\{\prod_{m=1}^{N}(\rho_m - z_m)\right\}\int_{-\infty}^{\infty}\frac{dR_x}{\prod_{j=1}^{N}(R_x - \rho_j)} \\ &\quad \times \exp\left\{-(R_x - R\sin\theta)^2\left(\frac{W}{2\cos\theta}\right)^2 + ixR_x + iz\left[R\cos\theta\right.\right. \\ &\quad \left.\left. -(R_x - R\sin\theta)\tan\theta + (R_x - R\sin\theta)^2/2R\cos^3\theta\right]\right\} \\ &= \frac{W_T}{2\pi^{\frac{1}{2}}\cos\theta}\left\{\prod_{m=1}^{N}(\rho_m - z_m)\right\}U^{(0)}(x,z)\exp\left\{\left(\frac{x_T}{W_T}\right)^2\right\} \\ &\quad \times\int_{-\infty}^{\infty}\frac{dR_x}{\prod_{j=1}^{N}(R_x - \rho_j)}\exp\left\{-\left[\frac{R_x - R\sin\theta}{2\cos\theta}\right]^2 W_T^2\right. \\ &\quad \left. + i(R_x - R\sin\theta)x_T/\cos\theta\right\} \end{aligned} \tag{21}$$

$$= \frac{W_m}{2\pi^{1/2}\cos\theta}\, U^{(0)}(x,z)\,(2R\cos\theta)^{1-N}\; I^{(N)} .$$

Here $I^{(N)}$ is the integral

$$I^{(N)} = \exp\left\{\left(\frac{x_m}{W_m}\right)^2\right\}\left\{\prod_{m=1}^{N}(\rho_m - z_m)\right\}\int_{-\infty}^{\infty}\frac{dK}{\prod_{j=1}^{N}(K-K_j)} \times \exp\left\{-(RW_mK)^2 + i2Rx_mK\right\}, \tag{22}$$

where

$$K = \frac{R_x - R\sin\theta}{2R\cos\theta} \quad , \quad K_j = \frac{\rho_j - R\sin\theta}{2R\cos\theta} .$$

$I^{(N)}$ can be evaluated analytically by using the convolution theorem in a manner like that employed by Pitts in treating the reflected beam. We first write

$$I^{(N)} = \left\{\prod_{m=1}^{N}(\rho_m - z_m)\right\}\exp\left\{\left(\frac{x_m}{W_m}\right)^2\right\}\int_{-\infty}^{\infty}F(y)\,G^{(N)}(b-y)\,dy , \tag{23}$$

in which

$$F(y) = \int_{-\infty}^{\infty}\exp\left\{-(RW_mK)^2\right\}\exp\left\{iyK\right\}dK = \frac{\pi^{\frac{1}{2}}}{RW_m}\exp\left\{-\left(\frac{1}{2RW_m}\right)^2 y^2\right\} \tag{24}$$

$$G^{(N)}(b-y) = \frac{1}{2\pi}\int_{-\infty}^{\infty}\frac{dK}{\prod_{j=1}^{N}(K-K_j)}\exp\left\{i(b-y)K\right\} . \tag{25}$$

$G^N(b-y)$ is integrable by complex contour integration. For $b > y$, the contour must enclose those poles with $\alpha_1,\ldots,\alpha_N > 0$ and for the $b < y$ case, it must enclose those with $\alpha_1,\ldots,\alpha_N < 0$. In forming both the approximations $T'(k_x)$ and $T''(k_x)$ only poles in the first quadrant were used. Therefore

$$G^{(N)}(b-y) = i \sum_{m=1}^{N} \left\{ \prod_{\substack{n=1 \\ n \neq m}}^{N} \frac{1}{K_n - K_m} \right\} \exp\{-i(b-y)K_m\}, \tag{26}$$

and the convolution integral can be carried through to yield

$$I^{(N)} = \exp\left\{\left(\frac{\chi_T}{W_T}\right)^2\right\} \sum_{m=1}^{N} \left\{(\rho_m - z_m)\left[\prod_{\substack{n=1 \\ n \neq m}}^{N} \frac{\rho_n - z_m}{K_n - K_m}\right] i\pi \exp\{\gamma_m^2\} \operatorname{erfc}(\gamma_m)\right\}, \tag{27}$$

where

$$\gamma_m = -\frac{\chi_T}{W_T} - i\frac{W_T(\rho_m - R\sin\theta)}{2\cos\theta}. \tag{28}$$

Finally the profile of the transmitted beam for the approximation T'', using N poles, is

$$U_{T''}^{(N)}(\chi, z) = U^{(0)}(\chi, z)\left[\frac{i\pi^{\frac{1}{2}}}{2\cos\theta}\right] W_T \sum_{m=1}^{N} \left\{(\rho_m - z_m)\left[\prod_{\substack{n=1 \\ n \neq m}}^{N} \frac{\rho_n - z_n}{R_\chi - \rho_m}\right] \times \exp(\gamma_m^2)\operatorname{erfc}(\gamma_m)\right\}. \tag{29}$$

The other approximation $T'^{(N)}(R_\chi)$ can be written as

$$T'^{(N)}(R_\chi) = 1 - \prod_{m=1}^{N}\left(1 + \frac{\rho_m - z_m}{R_\chi - \rho_m}\right) \tag{30}$$

To express $T'^{(N)}$ in terms of $T''^{(N)}$, Eq. (16) is rearranged to give

$$T''^{(N)}(\beta_x) = \prod_{m=1}^{N} \left(\frac{\rho_m - z_m}{\beta_x - \rho_m} \right) \tag{31}$$

Denoting $a_{m_\beta} = \frac{\rho_{m_\beta} - z_{m_\beta}}{\beta_x - \rho_{m_\beta}}$, it is noted from Eqs. (30) and (31) that

$$T'^{(N)}(\beta_x) = -\sum_{M=1}^{N} T_N''^{(M)}(\beta_x) \tag{32}$$

Where $T_N''^{(M)}(k_x)$ is defined as the sum of all possible products $a_{n_1} \ldots a_{n_M}$, in which n_k's can assume any value from 1 to N and must satisfy the requirement $a_{n_1} < a_{n_2} < \ldots < a_{n_M}$. For example, if N = 3, then $T_3''^{(1)} = a_1 + a_2 + a_3$, $T_3''^{(2)} = a_1a_2 + a_1a_3 + a_2a_3$, and $T_3''^{(3)} = a_1a_2a_3$. Insertion of Eq. (32) into Eq. (7) would lead to the transmitted beam profile corresponding to $T'^{(N)}(k_x)$,

$$U_{T'}^{(N)}(\chi, z) = -\sum_{M=1}^{N} U_{T_N''^{(M)}}^{(M)}(\chi, z), \tag{33}$$

where $U_{T_N''^{(M)}}^{(M)}(\chi, z)$ can be derived from Eq. (29).

V. Results and Conclusions

Theoretical predictions for these angles of incidence were obtained by numerically evaluating the transmitted beam profile $U_{T''}^{(N)}$ as given by Eq. (29). The approximation T'', Eq. (16) depends upon the complex poles $\rho_j = \beta_j + i\alpha_j$ of the transmission coefficient and, as shown by Pitts et al, $k_x = \beta_j$ corresponds to the condition for the existence of a vibrational mode of the plate. Since $k_x = k\sin\theta$, $\beta_j = k\sin\theta_j$ implies that at an angle of incidence θ_j the mode of vibration corresponding to the jth pole is excited. At an angle of incidence very near the jth pole, i.e.,

$$|\sin\theta_i - \sin\theta_j| < 0.03,$$

the contribution for the jth pole to the total intensity profile is five or more orders of magnitude greater than the contribution from other poles. At such angles the jth pole term dominates the entire expression for the transmission profile.

In our calculations, $U_{T'}^{(N)}(x,z)$ is used since poor agreement between $|T|$ and $|T''|$ is not tolerable in the determination of the transmitted profile. The transmitted profile was first calculated for the case where $\theta_i = \theta_j$. Because of the dominance of the jth pole, only that pole was accounted for in $U_{T'}^{(N)}(x,z)$ and the resulting profiles are shown in Fig. 2. The input values are chosen for a brass plate in water with fd = 2 MHz.mm and $\sin\theta_i = 0.36$ for two frequencies, 1 MHz and 7 MHz. The outstanding feature seen here is a lateral displacement of the transmitted beam relative to the incident beam. It is noted that in Fig. 2 the 7 MHz profile has a larger beam displacement but with a much lower intensity peak.

When there exist many poles in the neighborhood of $\sin\theta_i$, all the involved poles must be included in the evaluation of $U_{T'}^{(N)}(x,z)$ to obtain the appropriate profiles. For example, the transmitted profile was again calculated for a water-brass-water system with fd = 6.5 MHz.mm, f = 2MHz, and $\sin\theta_i$ varied from 0.31 to 0.36. In this angular range, there are two poles. The results of these calculations are shown graphically in Fig. 3. The profiles exhibit some interference effect and are seen to change with the incident angle.

The method employed in this work, while giving some reasonable results is limited in several ways. One is that the restraint (13) between R and T is bothersome and neither T' or T'', the forms of which are suggested partly by it, are fully satisfactory. A more serious limitation is the dependence of this method on the location of the poles of T; the closer $\sin\theta_i$ is to a particular p_j the better it works. A technique which does not involve the poles might be less restricted.

Acknowledgement:

Part of this work was supported by the Office of Naval Research, U.S. Navy. One of the authors (W.G.M.) gratefully acknowledges the cooperation by Prof. O. J. Leroy, Catholic University of Leuven, Kortrijk Campus, made possible through a Grant by NATO Scientific Affairs Division.

References

1. F. Goos and H. Hanchen, Ann. Physik 1, 333 (1947).

2. A. Schoch, Acustica 2, 1 (1952).

3. H.L. Bertoni and T. Tamir, Appl. Phys. 2, 157 (1973).

4. L.E. Pitts, "A Unified Theoretical Description of Ultrasonic Beam Reflections from a Solid Plate in a Liquid," Ph.D. Thesis, Georgetown Univ., Washington, DC (November, 1975).

5. K.W. Ng, "Non-Specular Ultrasonic Bounded Beam Transmission through Solid Plates," Ph.D. Thesis, Georgetown Univ., Washington, DC (December, 1979).

Figure Captions

1. Coordinate system and schematic diagram of a bounded beam reflected from and transmitted through a solid plate immersed in a liquid.

2. Intensity profiles calculated for a beam transmitted through a solid plate in water with fd = 2 MHz.mm and $\sin\theta_i$ = 0.36 for two frequencies: (a) 1 MHz and (b) 7 MHz.

3. Intensity profiles calculated for a beam transmitted through a solid plate in water with fd = 6.5 MHz.mm, f = 2 MHz, and $\sin\theta_i$ being varied from 0.31 to 0.36.

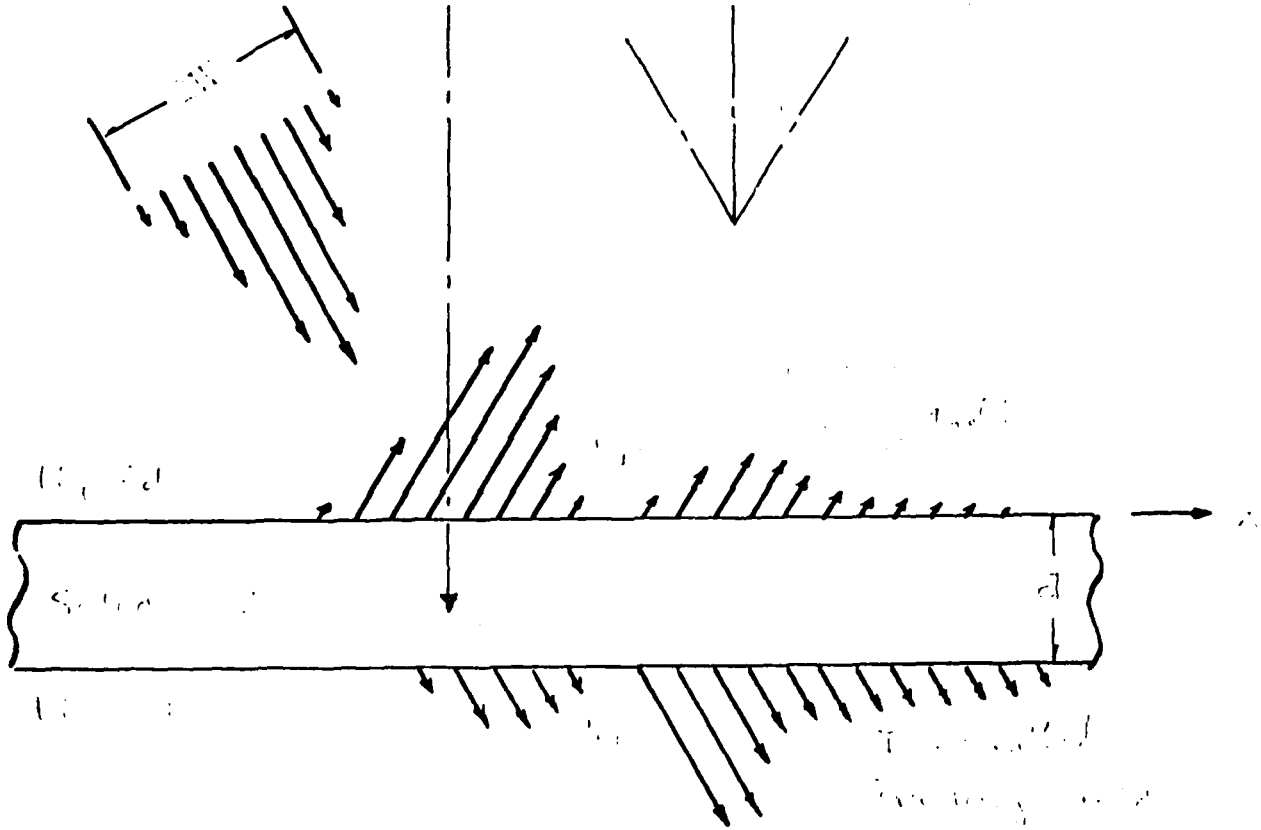

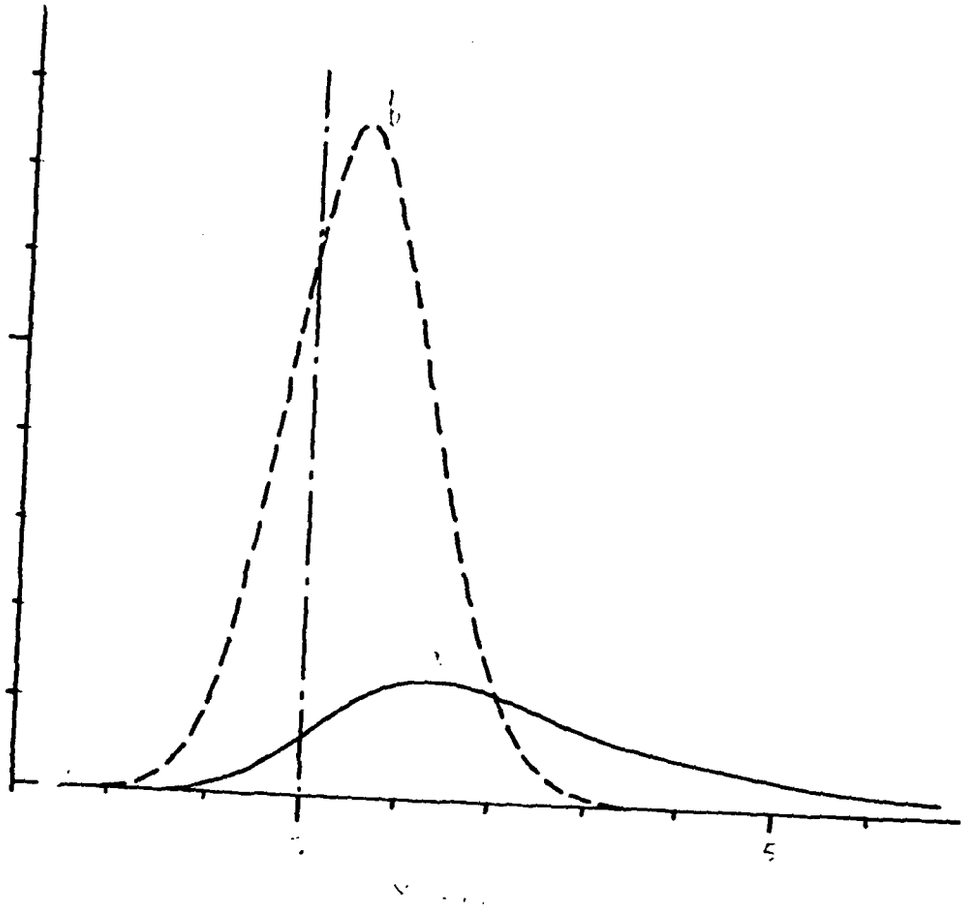

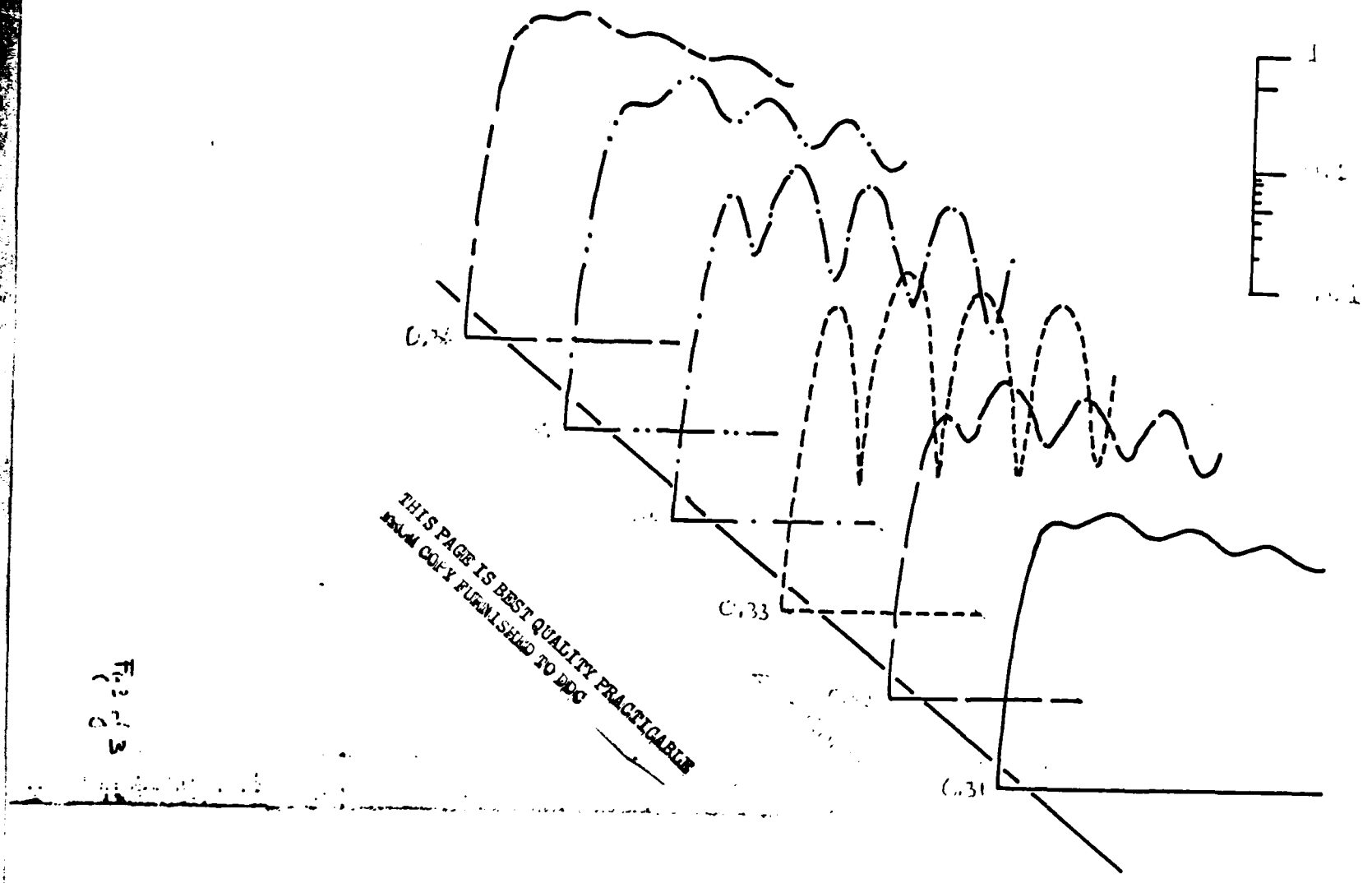

Correspondence

Restrictions on the Existence of Leaky Rayleigh Waves

NEAL G. BROWER, DOUGLAS E. HIMBERGER, AND WALTER G. MAYER

Abstract—The Rayleigh wave, an inhomogeneous surface wave, exists for all isotropic elastic solid infinite half-spaces. When the free surface of the solid is bounded by a liquid a leaky Rayleigh wave does not necessarily exist for all liquid/isotropic solid systems. The well-known condition for the existence of a leaky Rayleigh wave, the sound velocity in the liquid must be less than the shear wave velocity in the solid, is shown to be a necessary but not a sufficient condition. Additional conditions on density ratios and velocity ratios are given. Examples are listed showing liquid/solid combinations which satisfy the liquid-shear wave velocity condition but not the additional restrictions and thus do not support a leaky Rayleigh wave.

I. Introduction

The Rayleigh wave is a plane inhomogeneous surface wave which can propagate undiminished along the surface of an elastic half-space. The wave amplitude decreases exponentially normal to the surface. The existence of such surface waves, which can be supported by all elastic media, was shown by Lord Rayleigh [1].

There also exists surface waves for the case of a liquid/elastic solid system. One surface wave, the leaky Rayleigh wave, is an inhomogeneous wave which is damped along the interface formed by the adjoining two media. The damping is a manifestation of radiation into the liquid along the path of propagation. In the limit where the density of the liquid tends to zero, the leaky Rayleigh wave becomes a free Rayleigh wave. Unlike the free Rayleigh wave, the leaky Rayleigh wave does not exist for all real combinations of liquid/elastic solid media. A well-known example is an elastic solid in which the bulk shear wave velocity is less than the sonic velocity in the adjoining liquid.

Manuscript received April 2, 1979. This work was supported by the Office of Naval Research, U.S. Navy.

N. G. Brower was with the Physics Department, Georgetown University, Washington, DC 20057. He is now with the Johns Hopkins University Applied Physics Laboratory, Laurel, MD 20810.

D. E. Himberger and W. G. Mayer are with the Physics Department, Georgetown University, Washington, DC 20057.

The purpose of this paper is an investigation of further conditions on the existence of a leaky Rayleigh wave. The conditions involve restrictions on the following ratios which describe the liquid/elastic solid system: ρ_L/ρ_S, V_L/V_D, V_L/V_S, where ρ_L and ρ_S are the densities of the liquid and the solid, respectively, and V_L, V_D, and V_S are the sound velocity in the liquid, the longitudinal and shear bulk wave velocities in the solid.

Limits on these ratios are derived from numerical solutions of the secular equation for leaky Rayleigh waves and specific examples are given of liquid/elastic solid combinations which exceed the limits.

II. Theoretical Background

Consider an unbounded isotropic bulk medium. In this case two and only two different waves can be propagated. If the medium is bounded, other waves may exist.

A. The Rayleigh Wave

For an isotropic elastic solid with a plane boundary, a surface wave always exists. The wave is known as a Rayleigh wave. Briefly, one seeks a solution to the equations of motion for an elastic solid where the displacement amplitude decays exponentially perpendicular to the surface. At the boundary, all stress components must vanish. This leads to a secular equation for the velocity of the surface wave V. The secular equation is given by

$$4(V_S/V)^2[1-(V_S/V)^2]^{1/2}[(V_S/V_D)^2-(V_S/V)^2]^{1/2} + [1-2(V_S/V)^2]^2 = 0 \quad (1)$$

where V_D and V_S are the longitudinal and shear bulk wave velocities, respectively. There are three roots to the secular equation (1). The range of the Poisson ratio σ determines the nature of the roots. The Poisson ratio may be written in terms of the bulk velocities as

$$\sigma = (V_D^2 - 2V_S^2)/2(V_D^2 - V_S^2). \quad (2)$$

If the Poisson ratio is in the range where

$$\sigma < 0.263\cdots \quad (3)$$

then there exist three real roots to (1). However, if the Poisson ratio falls in the range where

$$\sigma > 0.263\cdots \quad (4)$$

0018-9537/79/0700-0306$00.75

there exist one real, and two complex conjugate roots. For all real media the Poisson ratio is bounded by

$$0 < \sigma < 0.5. \tag{5}$$

Complex roots are not acceptable for they imply attenuation or damping which is not the case for the free surface here. Further the root V must have a magnitude less than the velocity of the bulk shear wave in the medium,

$$V < V_S. \tag{6}$$

The constraint is a manifestation of the radiation condition. Thus there is only one root [2] satisfying (6). The root, given by

$$V = V_R \tag{7}$$

corresponds to the Rayleigh surface wave propagating with velocity V_R. The root (7) always exists. The Rayleigh velocity varies approximately from

$$0.87\ V_S \longrightarrow 0.96\ V_S \tag{8}$$

as the Poisson ratio varies from 0 to 0 5.

B. The Leaky Rayleigh Wave

Consider the elastic isotropic solid above, now loaded by a liquid half-space. Again one seeks a solution to the equations of motion in which the displacement amplitude attenuates exponentially normal to the interface. At the interface, normal stresses and displacements must be continuous. Further tangential stresses in the solid must vanish. Upon application of the boundary conditions, a new secular equation is derived. The secular equation is given by

$$\begin{aligned} &4(V_S/V)^2[1-(V_S/V)^2]^{1/2}[(V_S/V_D)^2-(V_S/V)^2]^{1/2} \\ &\quad + [1-2(V_S/V)^2]^2 + (\rho_L/\rho_S)[(V_S/V_D)^2 \\ &\quad - (V_S/V)^2]^{1/2}[(V_S/V_L)^2-(V_S/V)^2]^{-1/2} = 0 \end{aligned} \tag{9}$$

where V_L is the phase velocity in the liquid. The densities ρ_L and ρ_s correspond to those of the liquid and solid, respectively.

Two permissible roots exist for (9); one of them is real. This root always exists as in the Rayleigh wave case. The surface wave associated with this solution is known as the Stoneley wave. It is a pure surface wave propagating parallel to the interface without attenuation and exponentially damped in both directions normal to the boundary. The Stoneley phase velocity V_{ST} is constrained to be

$$V_{ST} < V_L. \tag{10}$$

There is a second root which is complex [3]. The value of this complex root approaches the Rayleigh wave velocity as the density of the liquid approaches zero. The inhomogeneous wave associated with the root is the leaky Rayleigh wave.

The complex root is an allowed solution for a liquid/elastic solid system. Attentuation implied by the complex nature of the root has physical meaning in this instance. As the leaky Rayleigh wave propagates, energy is transferred into the liquid. The real and the imaginary parts of the complex root,

$$\begin{aligned} V_{RR} &= \mathrm{Re}\ V \\ V_{RI} &= \mathrm{Im}\ V \end{aligned} \tag{11}$$

yield the phase velocity of the leaky Rayleigh wave and the attenuation, respectively.

C. Conditions for Existence of Leaky Rayleigh Wave

In contrast to the free Rayleigh wave, the leaky Rayleigh wave does not exist for all liquid/elastic solid plane half-spaces. A characteristic of the leaky Rayleigh velocity is

$$V_R \leq V_{RR} < V_S < V_D. \tag{12}$$

The value of V_{RR} must be less than the bulk shear velocity due to the radiation condition. Due to the loading by the liquid, the leaky Rayleigh wave velocity must be greater than the free Rayleigh wave velocity.

If the sonic velocity in the liquid exceeds the bulk shear wave velocity, then no leaky Rayleigh wave can be propagated. From consideration of the radiation condition again, the leaky Rayleigh wave velocity is constrained to

$$V_L < V_{RR}. \tag{13}$$

Thus, from (12) and (13), one obtains a necessary condition for existence of the wave, that is,

$$V_L < V_S. \tag{14}$$

This condition follows directly from Snell's law: for a surface wave radiating into the liquid, the direction of the radiation is given by

$$\sin\theta_L = V_L/V_{RR} \tag{15}$$

where for the surface wave, $\sin\theta_{RR} = 1$. If the liquid velocity exceeds the shear wave velocity, this implies that $V_L > V_{RR}$ or considering (15),

$$\sin\theta_L > 1. \tag{16}$$

The necessary condition (14) is well known; however, it is not the only condition necessary in order to admit a leaky Rayleigh wave solution. A second condition which encompasses the first is obtained through numerical analysis of (9).

III. Numerical Solution to Secular Equation

The secular equation (9) may be written as

$$\begin{aligned} &4(V_L/V)^2[(V_L/V_S)^2-(V_L/V)^2]^{1/2}[(V_L/V_D)^2 \\ &\quad - (V_L/V)^2]^{1/2} + [(V_L/V_S)^2 - 2(V_L/V)^2]^2 \\ &\quad + (V_L/V_S)^4(\rho_L/\rho_S)[(V_L/V_D)^2 \\ &\quad - (V_L/V)^2]^{1/2}[1-(V_L/V)^2]^{-1/2} = 0 \end{aligned} \tag{17}$$

for ease in calculation and consideration of the influence of the velocity and density parameters. Solutions to the leaky Rayleigh wave equation, (17), are obtained numerically. As a result of the calculation, it is seen that the existence of a leaky Rayleigh wave is dependent upon the ratios: V_L/V_D, V_L/V_S, and ρ_L/ρ_S. For given parameters V_L/V_D and V_L/V_S, the maximum allowable ρ_L/ρ_S is calculated. The results are tabulated in Table I. The limits on the Poisson ratio bound the relationship of the bulk shear wave velocity to the bulk elastic longitudinal wave velocity. Since the Poisson ratio has an upper limit of 1/2, the elastic bulk shear velocity, V_S, is given by

$$V_S < V_D/\sqrt{2}. \tag{18}$$

Due to this constraint the range of V_L/V_S is limited by the parameter V_L/V_D. This is expressed in Table I by the cutoff in calculated maxima in the density ratio.

As can be seen from Table I, as the bulk longitudinal wave velocity increases for a given shear wave and liquid velocity, the maximum density ratio increases. Likewise, as the elastic

TABLE I
MAXIMUM ALLOWABLE ρ_L/ρ_S AS A FUNCTION OF V_L/V_D (HORIZONTAL HEADING) AND V_L/V_S (VERTICAL HEADING)

	0.05	0.10	0.15	0.20	0.25	0.30	0.35	0.40	0.45	0.50	0.55
0.10	7.56										
0.15	4.87	5.36									
0.20	3.60	3.74									
0.25	2.83	2.89	3.05								
0.30	2.30	2.34	2.43	2.58							
0.35	1.93	1.96	2.01	2.09							
0.40	1.65	1.66	1.70	1.75	1.83						
0.45	1.42	1.43	1.46	1.49	1.55	1.60					
0.50	1.24	1.25	1.26	1.29	1.32	1.37					
0.55	1.08	1.09	1.10	1.12	1.14	1.18	1.21				
0.60	0.95	0.95	0.96	0.97	0.97	1.02	1.05	1.06			
0.65	0.83	0.83	0.84	0.85	0.86	0.88	0.90	0.92			
0.70	0.72	0.72	0.73	0.73	0.74	0.75	0.77	0.79	0.80		
0.75	0.62	0.62	0.62	0.63	0.63	0.64	0.66	0.67	0.69	0.70	
0.80	0.52	0.52	0.53	0.53	0.53	0.54	0.55	0.56	0.57	0.59	
0.85	0.43	0.43	0.44	0.44	0.44	0.45	0.45	0.46	0.47	0.48	0.50
0.90	0.30	0.30	0.30	0.31	0.31	0.32	0.32	0.33	0.33	0.34	0.35
0.95	0.22	0.22	0.23	0.23	0.24	0.24	0.25	0.26	0.27	0.27	0.29

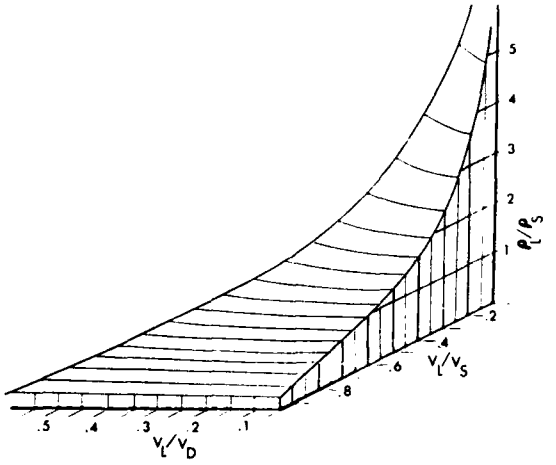

Fig. 1. Combinations of V_L/V_S, V_L/V_D, and ρ_L/ρ_S which allow propagation of a leaky Rayleigh wave. Points must lie within the volume shown for wave to exist.

shear velocity increases for given V_L and V_D, the maximum density ratio increases. Further, for constant V_D and V_S, i.e., for a given solid, an increase in the liquid velocity decreases the maximum allowable density ratio.

Fig. 1 shows the range of admissible parameter sets. All sets of the parameters under the curved surface yield a valid solution to (17). However, if for a given set of V_L/V_D and V_L/V_S the density ratio lies above the curve, then no leaky Rayleigh wave is possible. Thus one obtains the condition for existence of the leaky Rayleigh wave.

To illustrate the condition, several examples are given in Table II. For real media, there are cases where the velocity and density ratio parameters are such that no leaky Rayleigh propagation is possible. It is evident from Table II that there are cases where a leaky Rayleigh waves cannot be generated even if the usual condition ($V_L < V_S$) is satisfied.

TABLE II
EXAMPLES OF LIQUID ELASTIC SOLID COMBINATIONS WHICH FAIL THE EXISTENCE CONDITION

Liquid/Elastic Solid	V_L/V_D	V_L/V_S	ρ_L/ρ_S
Hg/Al	0.226	0.477	5.0
CCl_4/Lucite	0.346	0.842	1.35
Hg/Ni	0.265	0.485	1.53
Hg/Fused Silica	0.243	0.385	6.14
H_2O/Ice[4]	0.429	0.968	1.11

IV. CONCLUSION

The leaky Rayleigh wave, which is the complex solution to (9), approaches the Rayleigh wave as the density of the liquid goes to zero. While the free Rayleigh wave always exists, the leaky Rayleigh wave does not. It is well known that if the liquid velocity is greater than the bulk elastic shear wave velocity, then there is no admissible leaky Rayleigh solution. However, as a result of parametric investigation of the secular equation via numerical analysis a second set of conditions is evident. Existence of a solution does not only depend on V_L/V_S but on the values of the three ratios: V_L/V_D, V_L/V_S, and ρ_L/ρ_S.

REFERENCES

[1] J. W. Strutt, Lord Rayleigh, *The Theory of Sound* (Dover, New York, 1945), 2nd ed.
[2] I. A. Viktorov, *Rayleigh and Lamb Waves* (Plenum Press, New York, 1967).
[3] L. M. Brekhovskikh, *Waves in Layered Media* (Academic Press, New York, 1960).
[4] Y. Sato, Bull. Earthquake Res. Inst. Tokyo Univ. 29, 239 (1951).

JOURNAL DE PHYSIQUE

Colloque C8, supplément au n°11, tome 40, novembre 1979, page C8-175

ACOUSTO-OPTIC INTERACTION OF SECOND HARMONICS IN LAMB WAVES

N.G. BROWER and W.G. MAYER

Physics Department, Georgetown University, Washington, D.C. 20007

Résumé. - La possibilité de génération d'harmoniques d'ondes de Lambse propageant dans une plaque isotrope est examiné. Les conditions de la génération d'harmoniques sont discutées. Un système de détection utilisant l'intéraction acousto-optique permet de mettre en évidence l'existence de deuxièmes harmoniques en mesurant les disymétries de la figure de diffraction. Les résultats expérimentaux sont présentés.

Abstract. - The possibility of harmonic generation in Lamb waves propagating on isotropic plates is investigated. The conditions for harmonic generation are discussed. A detection scheme using the acousto-optic interaction is designed by which asymmetries in the diffraction pattern are measured to determine the existence of second harmonics. The results of the experiments are presented.

1. Introduction. - Finite amplitude mechanical vibrations in an elastic solid are nonlinear in nature which may give rise to a number of interesting interactions. One such interaction is the generation of harmonics as a finite amplitude acoustic wave is propagating in an elastic solid.

Acoustic bulk second harmonic generation was observed by Gedroits and Krasil'nikov[1]. When an initially monochromatic longitudinal ultrasonic bulk wave was launched in an elastic medium, a secondary longitudinal wave was observed. The second harmonic amplitude increased linearly with the interaction length, i.e., with the distance of travel.

Harmonic generation of acoustic surface waves in crystals was observed by Løpen /2/. His experimental results agreed with the theoretical analysis. As in the case of bulk waves, the amplitude of the second harmonic surface wave varied linearly with the interaction length and quadratically with the fundamental surface wave amplitude.

The possibility of harmonic generation in elastic isotropic plates is investigated in the present experiment. As an introduction, general features of second harmonic generation are presented as a theoretical background. Next, conditions for generation are discussed. The detection scheme utilizing a laser optical probe is outlined. A brief description of the experimental design is given. Finally results of the experiment are presented.

2. Theoretical Background. - Using a perturbative approximation /3/, the nonlinear equations of motion for an isotropic elastic solid bulk medium reduce to

$$\frac{\partial^2 \vec{U}}{\partial t^2} - C_L^2 \vec{\nabla} (\vec{\nabla} \cdot \vec{U}) + C_T^2 \vec{\nabla} \times \vec{\nabla} \times \vec{U} = \vec{Q}, \qquad (1)$$

where $\vec{U}$ is the particle displacement amplitude and C_L and C_T are the longitudinal and transverse bulk wave velocities. The term on the righthand side of eq.(1), $\vec{Q}$, is the source or forcing term. In the case of harmonic generation, $\vec{Q}$ consists of terms quadratic in the fundamental plane wave amplitude. An iterative solution/4/ to the nonlinear equation of motion yields

$$U_2 = C\, U_1^2\, x. \qquad (2)$$

The amplitude of the second harmonic, U_2, is proportional to the square of the fundamental wave amplitude, U_1, and also to the interaction length, x, with C a proportionality constant. This result is also obtained by Løpen /2/ for surface waves in which case U_1 is the fundamental surface wave amplitude. Similarly, for plate mode interactions, eq. (2) is valid, where U_1 is the Lamb mode fundamental amplitude. The characteristics implied by eq. (2) will be used to identify a generated harmonic.

In order that a harmonic be generated, the velocities of the fundamental and the harmonic must be equal, that is

$$v(\omega_1) = v(2\omega_1). \qquad (3)$$

This is a resonance condition. Two means of satisfying eq. (3) are possible for Lamb mode interaction. The curves in Fig. 1 show the Lamb mode velocity dispersion for an unloaded brass plate. One means of satisfying eq. (3) is by exciting a locally non-dispersive Lamb mode. For example, if the fundamental were excited at 7 MHz in the A_1 mode (point 1) then a second harmonic at 14 MHz (point 2) will satisfy the resonance condition. The resonance condition may also be satisfied for dispersive regions provided there is mode coupling. For example, consider a fundamental in the A_1 mode at 5 MHz (point 3) the second harmonic is in the A_2 mode (point 4). Whenever Lamb modes couple, eq. (3) is satisfied. This coupling has been observed by Brower and Mayer /5/ for the "isotropic three-phonon interaction".

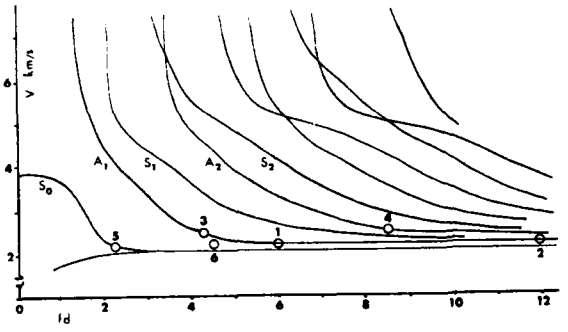

Fig. 1. - Velocity dispersion curves for a free brass plate as a function of product frequency times plate thickness (fd in units of MHz.mm). Selected points for harmonic generation are indicated by numbers 1 to 4 - see text.

The two cases of possible resonance are experimentally investigated here. Table I lists the fundamentals used and the possible harmonics generated.

TABLE I. Fundamental Lamb Modes and Harmonics

Fundamental Mode	Second Harmonic
A_1 at 7 MHz	A_1 at 14 MHz
A_1 at 5 MHz	A_2 at 10 MHz

3. Optical Detection of Second Harmonics. -

A. Basic Theory.

The optical detection system is based on the fact that a light beam (laser) will be diffracted upon reflection from a periodic surface corugation. This corrugation may be an acoustic surface wave (a Rayleigh wave) or a plate vibrational mode (a Lamb wave). A theoretical treatment of this acousto-optic interaction for a Rayleigh wave has been given by Mayer, Lamers, and Auth /6/. This treatment can be extended to include Lamb waves /7/. Fig. 2 is a schematic diagram of the laser-surface wave interaction. The light is incident into the surface at an angle ϕ and is diffracted into discrete diffraction orders with angular spacing θ, centered around the reflection angle ϕ. The light intensity in the mth diffraction order due to a single-frequency Lamb mode of amplitude U_1 is given by

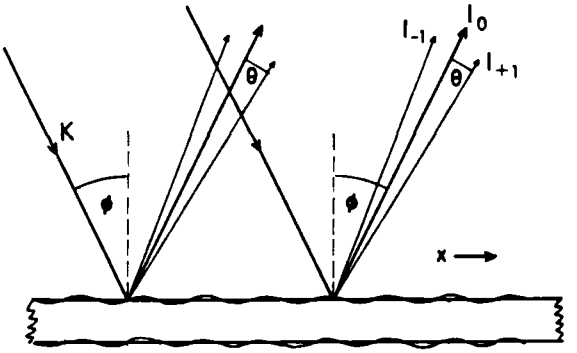

Fig. 2. - Schematic diagram for acousto-optic interaction caused by Lamb waves. K refers to the wave vector of the light incident at an angle ϕ, θ is the angular spacing of the first light diffraction order, and x denotes the direction of travel of the Lamb wave on the plate.

$$I_{\pm 1} = J_m^2(\gamma_1), \qquad (4)$$

where

$$\gamma_1 = 2KU_1 \cos\phi,$$

with K the wavenumber of the light and J_m the mth order Bessel function. It is evident from eq. (4) that the diffraction pattern is symmetric with respect to the central order reflected at angle ϕ.

Now consider a surface corrugation caused by a Lamb wave which, in addition to its fundamental

frequency, contains a second harmonic component of amplitude U_2. In this case the particle displacement will no longer be pure sinusoidal and a distorted Lamb wave will interact with the incident light beam. The resulting diffraction pattern will be asymmetric with respect to the central order. The amount of asymmetry will depend on the magnitude of U_2 relative to U_1.

This process is similar to that described by Neighbors and Mayer /8/ for nonsinusoidal Rayleigh waves. Using the same approach for nonsinusoidal Lamb waves and assuming that only the fundamental and a second harmonic component are present in the wave, the light intensities in the positive and negative first orders are given by

$$I_{+1} = [\ldots - J_3(\gamma_1)J_2(\gamma_2) - J_1(\gamma_1)J_1(\gamma_2) + J_1(\gamma_1)J_0(\gamma_2) - J_3(\gamma_1)J_1(\gamma_2) \ldots]^2 , \quad (5)$$

$$I_{-1} = [\ldots - J_3(\gamma_1)J_1(\gamma_2) - J_1(\gamma_1)J_0(\gamma_2) - J_1(\gamma_1)J_1(\gamma_2) - J_3(\gamma_1)J_2(\gamma_2) \ldots]^2 , \quad (6)$$

where $\gamma_2 = 2KU_2 \cos \phi$.

The series of products of Bessel functions in above equations can safely be truncated to the terms shown since both γ_1 and γ_2 are usually small so that insignificant errors in the values of I_{+1} and I_{-1} are introduced by neglecting terms in $J_r J_s$ with $r,s > 3$.

Equations (5-6) are the bases in the optical detection of the presence of second harmonics. If $U_2 \neq 0$, one finds that $I_{-1} > I_{+1}$, giving rise to an asymmetric diffraction pattern. It should be noted that eqs.(5-6) reduce to eq. (4) if $U_2 = 0$. In this case all terms vanish except $J_1(\gamma_1)J_0(\gamma_2)$ which equals $J_1(\gamma_1)$.

This analysis provides a method of determining the presence or absence of second harmonics in a vibrating solid plate. Probing the surface with a light beam and measuring the intensity distribution in the diffraction pattern yields information about the magnitude of U_2 compared to U_1. Moreover, probing the surface at different distances from the source of the Lamb wave generation, one can measure the change in harmonic content as a function of distance.

Due to the method of generating the fundamental Lamb mode, i.e., by means of the "liquid wedge" method /9/, the possibility exists that second harmonic components are generated in the liquid prior to incidence on the plate surface. However, if such components should be present and should continue to propagate along the plate they would at best decrease in amplitude as a function of distance traveled on the plate. Their amplitude could not increase as a function of distance on the plate unless harmonic generation on the plate is possible. Thus eq. (2) will be satisfied only if harmonic generation on the plate itself occurs. if harmonics propagate on the plate, asymmetry in the diffraction pattern will be observed ; to obtain numerical values, a new parameter, I_p, is introduced, defined as

$$I_p \equiv \frac{I_{-1} - I_{+1}}{I_{-1}} \times 100 \quad (7)$$

Using eq. (2), it may be shown that I_p is a linear function of distance from the source of the Lamb wave /7/ if the plate is considered to be a dissipationless medium. Therefore, I_p can be measured as a function of distance.

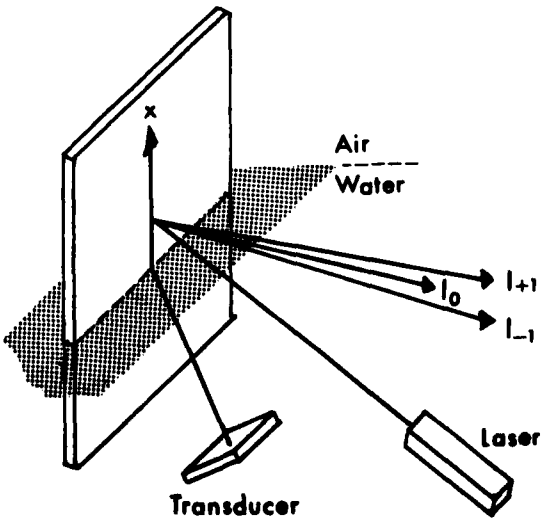

Fig. 3. - Experimental setup for optic probing of harmonic generation in Lamb waves.

B. Experimental Design and Results.

The design for the optical probing system is shown in Fig.3. Light from a He-Ne laser is expanded and collimated (details of the necessary optical components not shown in Fig. 3.) The collimated light beam is reflected from a highly polished brass plate which supports the Lamb wave. The diffracted-reflected light is focussed approximately 8 m from the plate. This distance is sufficient to properly separate the diffraction orders so that intensity measurements of I_{+1} and I_{-1} can be made with a photodiode.

Measurements of I_p were made at various distances x on the plate for the different fundamental frequencies and modes listed in Table I. Excitation of the modes was accomplished by adjusting the quartz transducer to the required angular position for the generation of the desired Lamb mode.

The polished brass plate, excited in the A_1 mode at 7 MHz, was probed with the He-Ne laser. A diffraction pattern was observed and the asymmetry between the first diffraction orders was measured. At a relative interaction length of 0.8 cm, the percent asymmetry was approximately 15%. The laser probe was then moved along the plate in the positive x-direction and the asymmetry increased. At a distance of 1.2 cm, a 29% asymmetry was observed. Likewise, for the plate in the fundamental A_1 mode, excited at 5 MHz, asymmetry was observed. In this case the asymmetry also increased with interaction distance. The results are listed in Table II.

TABLE II. I_p as a function of x.

x	I_p	
0.8 cm	15%	A_1 mode at 7 MHz
1.2 cm	29%	
0.9 cm	14%	A_1 mode at 5 MHz
1.3 cm	39%	

As a control, the S_0 mode at 3 MHz was excited (point 5 in Fig. 1.). As can be seen in Fig. 1., there is no second harmonic which satisfies Eq. (3) because the required location (point 6) does not fall on a curve. Therefore, there should be no second harmonic content in the detected mode. The measured diffraction pattern showed this to be true: no detectable asymmetry in the first orders could be found.

In conclusion, second harmonic generation in Lamb modes was detected. Harmonics were observed for both a locally dispersionless mode and also for the mode coupling case, provided the appropriate conditions for harmonic generation in plates were satisfied.

Acknowledgment. - This work was supported by the Office of Naval Research, U.S. Navy.

REFERENCES

/1/ Gedroits, A.A., and Krasil'nikov, V.A., Sov. Phys. JEPT 16 (1963) 1122.

/2/ Løpen, P.O., J. Appl. Phys. 39 (1968) 5400.

/3/ Jones, G.L., and Kobett, D.R., J. Acoust. Soc. Am. 35 (1963) 5.

/4/ Hikata, A., Chick, B.B., Elbaum, C., J. Appl. Phys. 36 (1965) 229.

/5/ Brower, N.G., and Mayer, W.G., J. Appl. Phys. 49 (1978) 2666.

/6/ Mayer, W.G., Lamers, G.B., Auth, D.C., J. Acoust Acoust. Soc. Am. 42 (1967) 1255.

/7/ Brower, N.G. Ph.D. Thesis (1976) Georgetown University, Washington, D.C.

/8/ Neighbors, T.H., and Mayer, W.G., J. Appl., Phys. 42 (1971) 3670.

/9/ Hallermeier, R.J., and Diachok, O.I., J. Appl. Phys. 41 (1970) 4763.

* Asymmetry will be influenced or be absent under certain conditions of the phase relation ship between the fundamental and the second harmonic, as pointed out by ALIPPI A., et al. J. Phys. 48 (1977) 2182.

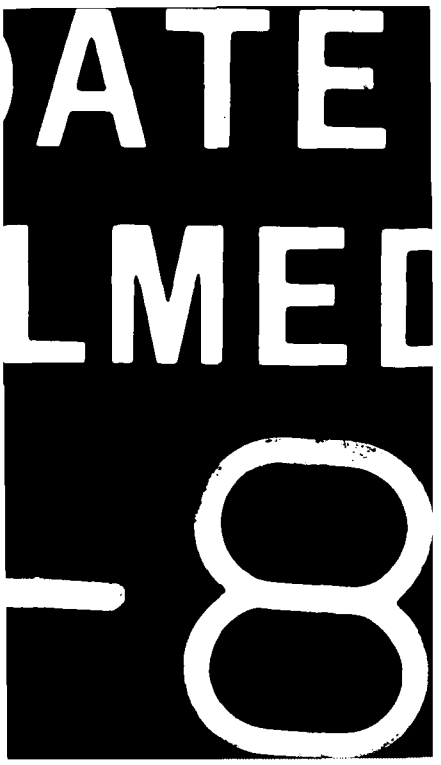
ATE
LMED
8